THE HILBERT TRANSFORM AND SEISMIC WAVELET PROCESSING

by

Kuo-An Lin

ProQuest LLC.
789 East Eisenhower Parkway
P.O. Box 1346
Ann Arbor, MI 48106 – 1346

ER-2096

A thesis submitted to the Faculty and the Board of Trustees of the Colorado School of Mines in partial fulfillment of the requirements for the degree of Master of Engineering in Geophysics.

Signed: Kuo-An Lin
Kuo-An Lin

Golden, Colorado

Date: July 31, 1978

Approved: Frank A. Hadsell
Frank A. Hadsell
Thesis Advisor

George V. Keller
George V. Keller
Head of Department
Geophysics

Golden, Colorado

Date: 21 August 1978, 1978

ABSTRACT

The thesis evaluates the effectiveness of time and frequency domain minimum-phase deconvolution techniques applied to seismic field wavelets.

Each of the wavelets was modeled using simulated or measured components, then each of the wavelets was deconvolved using Levinson's one-sided least-squares and Hilbert transform methods. The effect of white noise level in deconvolution filter design was evaluated.

The minimum-phase assumption should be met for the above two methods. Comparison of deconvolved outputs from the methods shows that the Hilbert transform approach is more suitable for wavelet deconvolution than the least-squares algorithm in those cases studied. The performance of Levinson's deconvolution degrades with increasing white noise level.

The deconvolved results show that the minimum-phase deconvolutions can restore the frequencies outside the central pass-band of the array response, but give time leads to the deconvolved wavelets of the array responses. Hence,

some of the desired signal energy in the recording filter band cannot be used effectively for velocity estimation.

TABLE OF CONTENTS

Table of Contents continued Page

LIST OF ILLUSTRATIONS

Page

Page

LIST OF SYMBOLS

Symbol	Definition
$A(f)$, $A(k)$	Fourier transform of receiver array response $a(t)$, $a(n)$
a_i	The coefficients of the time-domain operator
$\triangleq$	Equal as a matter of definition
f	Frequency in H_Z
Δf	The sampling interval in frequency domain
$h(t)$, $H(\omega)$	Analog functions for wavelet
$h(n)$, $H(k)$	Discrete functions for wavelet
$\hat{h}(t)$	Inverse Fourier transform of log $H(\omega)$
$\hat{hp}(n)$	Inverse Fourier transform of log $H(k)$
hz	Hertz
$I(k)$	Fourier transform of instrument filter $i(n)$
k	Frequency index
n	Time index
$n(t)$, $n_i(t)$	noise
N_s, n_s	white noise level
$r(t)$	Subsurface reflectivity function
rad	Radian
r_i	Autocorrelation coefficients
s	Laplace transform variable
$s(t)$	seismic trace
sec	second
t	time

Δt	The sampling interval in time domain
ΔT	The time duration of array response
$V_N(k)$	Discrete Hilbert transform kernel
$w(t)$	Seismic field wavelet
$w_i(t)$	Interpretation wavelet
ΔX	The length of receiver array
$\theta(k)$	Phase spectrom
$\delta(t)$	Impulse
ω	Angular frequency
$\Delta\tau$	The time interval between the elements of array.

ACKNOWLEDGEMENTS

The author wishes to express his sincere gratitude to Drs. Frank A. Hadsell and William A. Schneider of the Colorado School of Mines, who acted as advisors on this research project. Their many discussions and patient explanations are most deeply appreciated. Further thanks are given to Dr. William A. Schneider, who provided the raw data used in this project.

He is grateful to Drs. Maurice W. Major and Charles Stoyer of the Colorado School of Mines for serving as his committee members.

He is indebted to the Gulf Oil Corporation for providing one-year fellowship during his stay at the School.

Appreciation is also given to the Graduate School at the Colorado School of Mines for providing the numerous extensions of computer time necessary for the seismic data processing.

Special thanks are extended to his wife, Grace Show-Chin Ho, for her encouragement and patience in taking care of the family, in Taiwan, during his stay at the School.

INTRODUCTION

Petroleum seismograms are often effectively modeled mathematically according to

$$s(t) = w(t) * r(t) + n(t) \,,$$

where $s(t)$ is the seismic trace, $r(t)$ is subsurface reflectivity function, $n(t)$ is additive random noise, and $w(t)$ is called the field wavelet.

A practical objective of seismic wavelet processing is to transform the field wavelet into an interpretation wavelet as illustrated below

$$s(t) \rightarrow \boxed{\text{seismic processing}} \rightarrow w_i(t) * r(t) + n_i(t) = \underline{s}\ (t).$$

Here $w_i(t)$ is the interpretation wavelet, and supposedly $\underline{s}\ (t)$ is more easily interpreted than $s(t)$.

Recently, wavelet deconvolution techniques have taken on new importance as exploration has entered the stratigraphic era.

Wavelet deconvolution includes the techniques of estimating and shaping the field wavelet; but practicing interpretors agree that the bandwidth of $w_i(t)$ should be substantially

greater than that of w(t) and that the phase shift of $w_i(t)$ should be less than that of w(t), and approach zero phase as an ultimate goal.

The traditional approach to these objectives has been statistical deconvolution based on the Weiner filter, designed from the autocorrelation function in the time domain. A discussion of the general properties of the digital Wiener filter has been given by Robinson and Treital (1967). Peacock and Treitel (1969) have demonstrated that Wiener filter can be identified as the unit prediction error operator.

Another approach to wavelet processing is based on the Hilbert transform, in the frequency domain. As described by Robinson (1967), the phase spectrum of an input wavelet can be computed from the input logarithmic power spectrum if the minimum-phase assumption is satisfied. A further mathematical analysis of the approach has been given by Oppenheim (1975).

The objective of this thesis is to evaluate the relative effectiveness of these two deconvolution techniques.

Throughout this thesis the Oppenheim (1975) philosophy is adopted. Very briefly, this is that the given time series has a physical significance but the nature of this significance is not to be analyzed carefully. In particular the time series under consideration here are purported to represent analog processes. This is a common point of view in modern engineering data processing.

THE TIME DOMAIN DECONVOLUTION

Since 1957 (Robinson, 1957), least-squares inverse filters have been used for wavelet deconvolution. Numerous author discussed this time-domain deconvolution approach in which one solves normal equations in order to obtain the deconvolution operator. The normal equations can be solved using Levinson's algorithm (Levinson, 1946).

In this thesis, the following matrix equation will be solved to obtain a prediction operator,

$$\begin{bmatrix} r_0 & r_1 & \cdots & r_{n-1} \\ r_1 & r_0 & \cdots & r_{n-2} \\ & & \vdots & \\ r_{n-1} & r_{n-2} & \cdots & r_0 \end{bmatrix} \begin{bmatrix} a_0 \\ a_1 \\ \vdots \\ a_{n-1} \end{bmatrix} = \begin{bmatrix} r_1 \\ r_2 \\ \vdots \\ r_n \end{bmatrix} , \quad (1)$$

where r_i is the autocorrelation of the input wavelet, (a_0, a_1,..., a_{n-1}) is the prediction operator with prediction distance unity and length n.

Equations (1) may be rearranged as

$$\begin{bmatrix} r_0 & r_1 & \cdots & r_n \\ r_1 & r_0 & \cdots & r_{n-1} \\ & & \vdots & \\ r_n & r_{n-1} & \cdots & r_0 \end{bmatrix} \begin{bmatrix} 1 \\ -a_0 \\ \vdots \\ -a_{n-1} \end{bmatrix} = \begin{bmatrix} \beta \\ 0 \\ \vdots \\ 0 \end{bmatrix}, \quad (1\text{-}1)$$

(Peacock, 1969)

where β is a scale factor, $(1, -a_0, \ldots, -a_{n-1})$ is the unit prediction error operator, which is equivalent to the least-squares deconvolution filter which ideally transforms an unknown input wavelet to an impulse at zero delay (Peacock, 1969).

For the time-domain deconvolution, the minimum-phase characteristic of the input wavelet ensures that the one-sided inverse filter is stable.

Experience has taught us that the effectiveness of the unit prediction error operator increases with increasing filter length n, but the effectiveness is no longer improved when the filter length increases beyond a certain value.

The deconvolved wavelets obtained by use of this one-sided least-squares approach should be similar to those

obtained by using the Hilbert transform, since both methods are determined using the autocorrelation (equivalently the power spectrum) and, as we shall see, require the minimum-phase assumption.

THE HILBERT TRANSFORM METHOD

For a seismic wavelet, h(t), we can express the logarithm of the wavelet's Fourier transform as

$$\hat{H}(\omega) \triangleq \log H(\omega) = \log |H(\omega)| + j\arg(H(\omega)), \qquad (2)$$

where j is the imaginary number ($\sqrt{-1}$).
The inverse Fourier transform, h(t), of log $H(\omega)$ can be written

$$\hat{h}(t) = \hat{he}(t) + \hat{ho}(t), \qquad (3)$$

where $\hat{he}(t)$ and $\hat{ho}(t)$ denote the even and odd parts of $\hat{h}(t)$. The even part $\hat{he}(t)$ is the inverse Fourier transform of log $|H(\omega)|$.

H(s), defined on the s-plane, is not, in general, analytic and might have poles and zeros which are branch points of log H(s). Hence, log H(s) must be made into a single-valved function by defining branch cuts before meaningful analyses may be conducted. If we assume that H(s) is analytic and has no zeros for Res $\geq$ 0, then log H(s) will also be analytic in the right-hand plane and arg (H(s)) can be uniquely determined from log $|H(s)|$ as we shall show below.

Given the applicability of Jordan's lemma and the above mentioned analyticity in the right half plane, the implied casuality of $\hat{h}(t)$ requires that

$$\hat{h}o(t) = \hat{h}e(t)\ \mathrm{sgn}(t), \tag{4}$$

where

$$\mathrm{sgn}(t) \triangleq \begin{cases} -1 & t<0 \\ 1 & t>0 \end{cases}.$$

Hence, equation (3) becomes

$$\hat{h}(t) = \hat{h}e(t)\ [1 + \mathrm{sgn}(t)] \tag{5}$$

Equation (5) is an expression of analog casuality.

Using the transform pair

$$1/jw \longleftrightarrow 1/2\ \mathrm{sgn}\ (t)$$

we may write the Fourier transform of equation (5) as

$$\hat{H}(\omega) = \log |H(\omega)| + j \log |H(\omega)| * -2/\omega \tag{6}$$

From equations (2) and (6), we obtain a minimum phase

$$\arg\ (H(\omega)) = \log |H(\omega)| * -2/\omega \tag{6-1}$$

Consequently, the Hilbert transform kernel $-2/\omega$ can be used to find the minimum phase $\arg\ (H(\omega))$ from $\log |H(\omega)|$.

Computation of the Digital Hilbert Deconvolution Operator

We must employ the discrete Fourier transform because our data is sampled and we do the analysis on a digital computer, therefore, the above analogue results are only of academic interest.

With the discrete fast Fourier transform, the computation of the Hilbert transform becomes very fast. To obtain an efficient algorithm for designing the digital deconvolution operator, we will look at the Hilbert transform relations for discrete data.

The discrete version of Eq. (2) can be written as

$$\hat{H}p(k) \triangleq \log H(k) = \log |H(k)| + j \arg (H(k)), \qquad (7)$$

$$k = 0, 1, \ldots, N,$$

and the inverse Fourier transform of $\hat{H}p(k)$ will be denoted as $\hat{h}p(n)$.

N should be chosen to be at least the length of the input sequence h(n). The fast Fourier transform requires that N be equal to 2^m (m: integer).

For the sake of expediency within the computer both $\hat{H}p(k)$ and $\hat{h}p(n)$ are defined as periodic sequences of period N. Their relation to "reality" is that $\hat{h}(n) = \hat{h}p(n)$ over $n = 1, \ldots, N/2 - 1$. (see below). Hence, we can, with a suitable definition of casuality, relate the real and the imaginary of the discrete Fourier transform of $\hat{h}p(n)$ in a manner similar to that devloped for $\hat{h}(n)$.

We can express the $\hat{h}p(n)$ as the sum of the even sequence $\hat{h}pe(n)$ and the odd sequence $\hat{h}po(n)$. A periodic sequence cannot be casual. However, as shown by Oppenheim (1975), we can define

a "casual" periodic sequence to be one for which $\hat{hp}(n) = 0$ for $N/2 < n < N$. Because of the periodicity of $\hat{hp}(n)$, $\hat{hp}(n) = 0$ for $-N/2 < n < 0$. Oppenheim (1975) points out that for finite-length sequences, we interpret this restriction to mean that the sequence is considered to be of length N, when in fact the last half of the points are zero. Consequently, $\hat{hp}(n)$ can be shown to be expressible as

$$\hat{hp}(n) = \hat{hpe}(n) \cdot u_N(n), \quad n = 0, 1, \ldots, N-1 \qquad (8)$$

here

$$u_N(n) \triangleq \begin{cases} 1, & n = 0, N/2 \\ 2, & n = 1, 2, \ldots, (N/2) - 1 \\ 0, & n = (N/2 + 1), \ldots, N-1. \end{cases}$$

The discrete Fourier transform of $u_N(n)$ is

$$U_N(k) = \begin{cases} N, & k = 0 \\ -j2\cot(\pi k/N), & k \text{ odd} \\ 0, & k \text{ even} \end{cases}$$

(Oppenheim, 1975)

Hence, we can express the distrete Fourier transform of equation (8) as

$$\hat{Hp}(k) = \log \left| H(k) \right| + j/N \sum_{m=0}^{N-1} \log \left| H(m) \right| V_N(k-m) \qquad (9)$$

here

$$V_N(k) = \begin{cases} -2\cot(\pi k/N), & k \text{ odd} \\ 0, & k \text{ even} \end{cases}$$

Equations (7) and (9) imply that the phase can be computed from the amplitude as

$$\arg\,(H(k)) = 1/N \sum_{m=0}^{N-1} \log \left| H(m) \right| V_N(k-m), \qquad (9\text{-}1)$$

A comparison of the development leading to equation (6-1) with that leading to equation (9-1) shows why the convolution of (9-1) is referred to as the discrete Hilbert Transform.

Using the concepts of this section, it is possible to construct the entire trnasform $\hat{H}p(k)$ from the logarithm of amplitude. Probably the simplest way to do this is as follows:

1. Take the discrete inverse Fourier transform of log $\left| H(k) \right|$ and so obtain $\hat{h}pe(n)$;

2. Multiply $\hat{h}pe(n)$ by $u_N(n)$, which according to equation (8), is $\hat{h}p(n)$;

3. Take the discrete Fourier transform of $\hat{h}p(n)$. The real part of this final results is log $\left| H(k) \right|$ and the imaginary part is an approximation to the minimum phase. Hence, if the input wavelet h(n) is minimum-phase, and if N is adequately large, then the computed phase (9-1) will approach the input minimum phase.

Even for large N, the computed phase can be expected to differ slightly from arg (H(k)) because the $\hat{h}p(n)$ may be an aliased sequence. If the input wavelet is non-minimum-phase, then the computed phase cannot be equal to arg (H(k)).

The designed deconvolution operator for a minimum-phase input wavelet should be

$$H^{-1}(k) = |H(k)|^{-1} \exp(-j \arg(H(k))), \qquad (10)$$

The sequence of operations used to obtain a deconvolved wavelet using the discrete, periodic Hilbert transform of this section is shown in Figure 1.

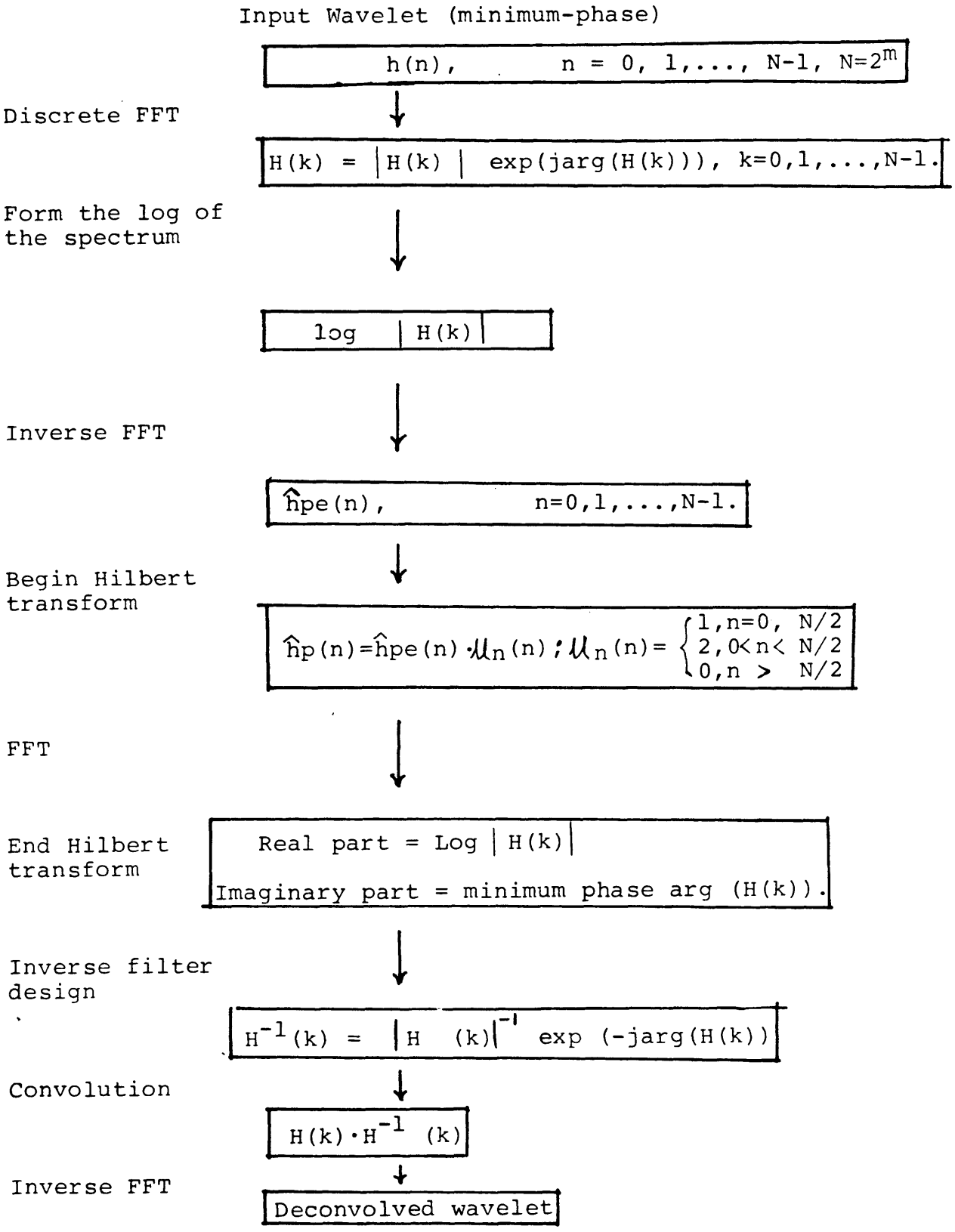

Figure 1. The Frequency-Domain Deconvolution

MINIMUM-PHASE ASSUMPTION

The minimum phase of a wavelet ensures that most of the energy in the wavelet will be concentrated in the front of the wavelet. The inverse of the minimum-phase wavelet is also a minimum-phase wavelet. The minimum-phase inverse wavelet can be employed as a stable causal convolution operator.

Many different signals can have the same auto-correlation function (equivalently the power spectrum). Given an amplitude spectrum for a wavelet of length n+1, there are 2^n wavelets with different phase spectra which will have this amplitude spectrum (Lines, 1977). Only one of these wavelets is minimum phase. In the application of inverse filtering, it is often necessary to obtain an appropriate phase curve given only an autocorrelation function (or a power spectrum). The significance of the minimum-phase is that it is uniquely derivable from the given autocorrelation function (or power spectrum).

In the section on the Hilbert Transform Method, the analog expression (Equation (6)) of the Hilbert transform is derived from the minimum-phase assumption for the input

wavelet h(t). In the discrete case (Equation (9)), the requirement that log $|H(k)|$ and arg $|(H(k))|$ be a discrete Hilbert transform pair is often referred to as the minimum-phase condition (Oppenheim, 1975) even though such is not the case except for arbitrarily large N.

The minimum-phase condition is that there are no poles or zeros inside the unit circle in the Z-plane, hence the minimum-phase function is analytic in this region. All zeros, as well as the poles of the function must lie outside the unit circle. (Here we are using $Z=e^{-s\Delta t}$, not $Z=e^{s\Delta t}$). Consider the Z-tranform expression of Equation (7). The functions log $|H(Z)|$ and arg (H(Z)) are a Hilbert transform pair if the region of convergence of $\hat{Hp}(Z)$ includes the unit circle and $\hat{Hp}(Z)$ is analytic in this region (Oppenheim, 1975). Since $\hat{Hp}(Z)$ can be divergent at both the poles and the zeros of H(Z), we require that there are no poles or zeros of H(Z) on or within the unit circle; i.e., that h(n) is minimum phase.

In summary, the processes of the minimum-phase deconvolutions, both that using the Hilbert transform method and that using the one-sided least-squares algorithm, lean heavily on the minimum-phase assumption in the development of the inverse operator. Theoretically, for minimum-phase input wavelets, both methods should give a Dirac impulse output. For the non-minimum-phase input, the amplitude spectrum of

deconvolved output may be whitened, which may improve resolution, but the phase of the output will be mixed causing relative errors in reflection travel time and interpretations based thereon.

WHITE NOISE

Relations to Deconvolved Amplitude

The amplitude of seismic signal decreases from low to high frequencies and eventually the amplitude of the noise will be higher than that of the signal. Deconvolution inverts the amplitude spectrum of the input tra ce and hence, will produce an output in which the high-frequency noise dominates the low-frequency signals. A way of solving this problem is to add a constant, which is often called white noise, to the input power spectrum during the frequency-domain operator design.

$$\text{The amplitude of the operator} = \frac{1}{\sqrt{|H(k)|^2 + N_s(k)}}, \qquad (11)$$

where $|H(k)|$ is the amplitude spectrum of the input wavelet and $N_s(k)$ is the added white noise.

In the time-domain deconvolution, we add the constant to the zero-lag term of the autocorrelation function of the wavelet during the time-domain operator design. After the white noise constant is added, the normal equations (1) used to compute the prediction operator will become

$$\left(\begin{bmatrix} r_0 & r_1 & \cdots & r_{n-1} \\ r_1 & r_0 & \cdots & r_{n-2} \\ \cdot & & \cdot & \\ \cdot & & \cdot & \\ \cdot & & \cdot & \\ r_{n-1} & r_{n-2} & \cdots & r_0 \end{bmatrix} + n_s r_0 I \right) \begin{bmatrix} a_0 \\ a_1 \\ \cdot \\ \cdot \\ \cdot \\ a_{n-1} \end{bmatrix} \begin{bmatrix} r_1 \\ r_2 \\ \cdot \\ \cdot \\ \cdot \\ r_n \end{bmatrix}, \quad (12)$$

where I is an identify matrix and n_s is white noise.

The addition of white noise provides an input power spectrum which is only slightly different in the spectral range of interest and which goes to zero nowhere. Thus it imparts an artificial stability to a process which is, at best, metastable. Usually, the constant will be 0.01 percent to 10 percent of the zero-lag value, depending upon the quality of the data.

The amplitude spectrum of the transform of a single spike in the time domain is a constant over the entire frequency spectrum. The addition of a white noise constant to the zero-lag term of the autocorrelation will raise all power spectrum values by a uniform amount. By definition, white noise is of infinite band-width and non-correlative. The autocorrelation of white noise is a single spike. Therefore, the amplitude spectrum of white noise is identical to that of a single spike. Consequently, the addition of a constant to the zero-lag term of autocorrelation is equivalent to the addition of a constant to all components of the power spectrum.

Influence on Phase Computation

The addition of the white noise constant is not always essential when computing the phase of the operator. For the Hilbert transform, the minimum-phase curve is computed independently by convolving the logarithm of the amplitude spectrum with $V_N(k)$ as described in Equation (9-1). For most minimum-phase input wavelets, the zeros of the input wavelet are sufficiently removed from the unit circle, that it is not necessary to add a constant into $\log |H(k)|$ to prevent its divergence.

From Equation (12), it can be seen that the addition of the white noise constant to the normal equations will effect both the phase and the amplitude of the operator.

Spectrum Editing

Equation (9-1) illustrates that the computed phase at any frequency is a function of the amplitude at all other frequencies because of the convolutional relationship. In particular, regions of low power become, after taking the logarithm, large negative values, and have considerable influence on the computed phase at all frequencies. Therefore, it is extremely critical to estimate the notches in the amplitude or power spectrum in order to compute the correct minimum-phase spectrum. In the frequency domain, sometimes this is fairly easy to do, since the roll-off slopes and notch

characteristics are often known for many of the wavelet components (Schneider, 1977).

ZERO-PHASE BANDPASS FILTER

For the purpose of removing noise not adequately suppressed by adding white noise in the deconvolution operator design, the deconvolved wavelet must pass through a zero-phase band-pass filter after deconvolution. In this thesis a zero-phase filter is a filter whose phase is an integer multiple of π except at a set of spectral points of measure zero. The band-pass filter is a dominant factor in determining the interpretation wavelet. To the extent that deconvolution flattens the spectrum, the amplitude spectrum of the deconvolved wavelet is that of the band-pass filter (M. Schoenberger, 1974).

COMPUTATIONAL RESULTS

The seismic field wavelets deconvolved in the study are presented in two parts. The wavelets in part A include source signature, ghost response, instrument response, and the combination of the above wavelets. That in part B is array response.

Before deconvolution, the input wavelet was delayed 100 points. After deconvolution the wavelet was advanced 100 points, then the deconvolved phase was computed.

The unit for all of the amplitude spectra is percent; that for all of the phase spectra is the radian.

Part A. Source Signature, Ghost Response, and Instrument Response

In this part, each wavelet was deconvolved both by applying the Hilbert transform and Levinson's algorithm. For each wavelet, the input wavelet and its Fourier spectra are shown in the first figure, e.g. 2A. The deconvolved results including output wavelets (2B), minimum-phase estimates of the input wavelet (2C), output amplitude spectra

(2D) and deconvolved phases (2E) are shown in the subsequent figures. The results obtained by the Hilbert transform are shown at the top of each labeled figure, those obtained by Levinson's method are at the bottom.

Input parameters are:

The number of sampled points for FFT	512 points
Sampling interval	
Time domain	0.002 or 0.001 sec.
Frequency domain	1/(512 x 0.002) or 1/(512x0.001) hz
Operator length	
Time domain	151 points
Frequency domain	512 points
White noise level	0.01%

The first example (Figure 2A) is a measured marine Aquapulse signature. The deconvolved signature (Figure 2B) was passed through a zero-phase band-pass filter in order to remove the high-frequency components generated during the deconvolution operation. The deconvolved wavelets obtained both by using the frequency-domain and the time-domain techniques are quite similar and zero-phase. Also, both of the minimum-phase estimates (Figure 2C) are quite similar to the input (Figure 2A). The deconvolved amplitude spectra (Figure 2D) are whitened, and the output phase errors (Figure 2E) are small. Because of the improper sampling for the

impulse response of the signature, the scrambling of the amplitude spectrum content due to aliasing appears in Fig. 2A-b. However, the quality results of Fig. 2B and 2C were obtained due to the minimum-phase characteristic of the sampled response, as we shall describe below.

The deconvolved results for a ghosting filter (Figure 3A) are shown in Figure 3B to 3E. Again, we can observe that both of the deghosted responses (Figure 3B) are zero-phase and the two estimates (Figure 3C) behave like the original waveform.

The third example is a 8/18-62 hz recording filter (Figure 4A). Before going through the Hilbert transform, the input amplitude spectrum was edited so that it had the deep notch at the zero frequency, with roll-off slope of 18 db/octave, as specified above, in order to simulate the known recording filter response on the low side. The frequency-domain deconvolution technique produced the nearly symmetric output wavelet (Figure 4B, top) but the time-domain method, for which only simple "white noise" editing is practical, gave the non-symmetric output (Figure 4B, bottom). Figure 4C shows the two minimum-phase estimates of the impulse response, that obtained by using the Hilbert transform is more similar to the original input wavelet (Figure 4A) than that obtained by Levinsons' method.

Figure 5A shows the response of a composite system made up of the airgun, the free surface (ghost reflector) and the recording system. Figure 6A is a 20 cu. in. airgun signature. The similar technique of editing the low-frequency portion of the input amplitude spectrum was applied to the above two wavelets before passing the amplitude spectrum through the Hilbert transform. The Hilbert transform deconvolution provided the nearly symmetric output pulses (Figure 5B and 6B, top) and the input-waveform estimates (Figures 5C and 6C, top). However, the one-sided least-squares scheme gave the different ones.

Discussion of the Results in Part A

1) Phase characteristics of the wavelets

The estimate of the input wavelet is obtained by inverting the operator, which is the inverse of the input wavelet. The inverse of a minimum-phase wavelet is also a minimum-phase one. Consequently, the zero-phase of symmetric characteristic of the deconvolved pulse and the closeness between the input and its estimate imply that the input is minimum-phase, or at least nearly so.

Figure 2B and 3B show the deconvolved Aquapulse signature and the deghosted response are very nearly zero-phase pulses centered on the onset of the original input. The minimum-phase estimates (Figures 2C and 3C) both for the

Aquapulse signature and the ghost response have remarkable agreement with the correspondent input wavelet. The minimum-phase condition is met by the above two wavelets. The symmetric characteristics of deconvolved waveforms and the minimum-phase estimates for the 8/18-62 hz recording filter, the composite system and the 20 cu. in. airgun signature imply that the wavelets are very nearly minimum-phase. Consequently, we can draw the conclusion that the minimum-phase assumption for the seismic field wavelets is quite reasonable or that these methods are surpriseingly insensitive to deviations from the optimum phase lag; i.e., minimum.

2) Comparison of effectiveness of the two methods

During inverse filtering we add the input phase to its negative and multiply the input amplitude by its inverse, thus requiring that the output be zero-phase or symmetric, and the output amplitude be flat. An effective deconvolution procedure should produce seismic wavelets with (a) a zero-phase spectrum, and (b) a smooth and broad amplitude spectrum. In Figure 2D and 3D, the deconvolved amplitude spectra obtained by the Hilbert transform is flatter than that obtained by the time-domain method, for the same white noise level of 0.0001.

Figures 4B, 5B, and 6B indicate that the deconvolved wavelets by the frequency-domain technique are more symmetrical than those by the time-domain method.

Figures 4C, 5C, and 6C indicate that the estimates by use of the Hilbert transform are closer to the corresponding input than those by Levinsons' scheme.

Thus, we can say that the Hilbert transform is more suitable for seismic wavelet processing than the time-domain approach. Galbraith (1971) points out that the Hilbert transform and the Levinson's approach would be the equivalent if an infinite number of inverse filter points could be used in the Levinson's method. Besides, in the frequency-domain deconvolution we can compute the minimum phase, employed in the inverse filter design, from an edited amplitude spectrum. Equivalent editing of auto correlations, as would be required if the least-squares method were used exclusively, would require an uncommon appreciation of the implication of autocorrelations or two additional Fourier transforms.

3) Evaluation of the effect of white noise

Figures 7B and 7C are examples used for evaluating the effect on deconvolution of adding a white noise constant to the impulse response of the DFS IV 8/36-32 hz recording filter (Figure 7A). The spectrum editing technique was also applied to minimize the effect of the deep notch at zero frequency with roll-off slope of 36 db/octave. Hence, the Hilbert transform produced the nearly symmetric output pulses (Figure 7B); the one-sided least-squares scheme gave the

nonsymmetric outputs (Figure 7C). As shown in Figures 7B and 7C, the white noise level has no influence on the deconvolved phase for the frequency-domain deconvolution; but markedly influences the degree of apparent stabilization of output pulse for the time-domain deconvolution. The performance of the one-sided least-squares deconvolution degrades with increasing white noise level. The zero-phase band-pass filter was not applied to the raw deconvolved outputs in Figures 7B and 7C, thus, it can be seen that increasing the white noise level can suppress the noise generated during the deconvolutions.

The processed wavelets (Figure 7D) and estimated waveforms (Figure 7E) demonstrate that the spectrum editing is extremely important when computing the correct phase curve used in operator design. If one ignores such a notch it may invalidate his phase calculation. It is much harder to ignore such a notch if one is using the Hilbert transform.

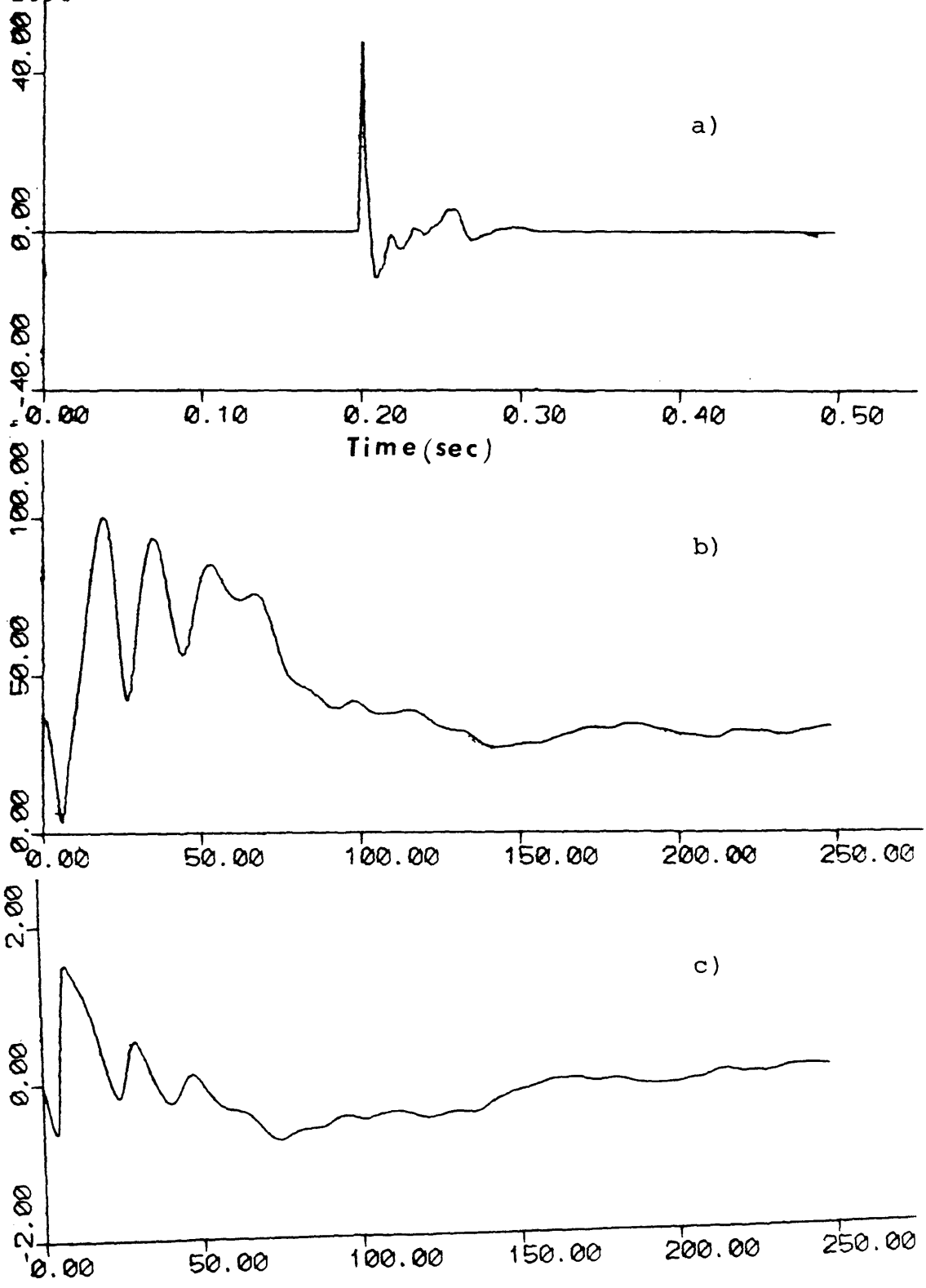

Figure 2A. Pressure signature from Aquapulse source
a) Impulse response, b) Amplitude spectrum. c) phase spectrum

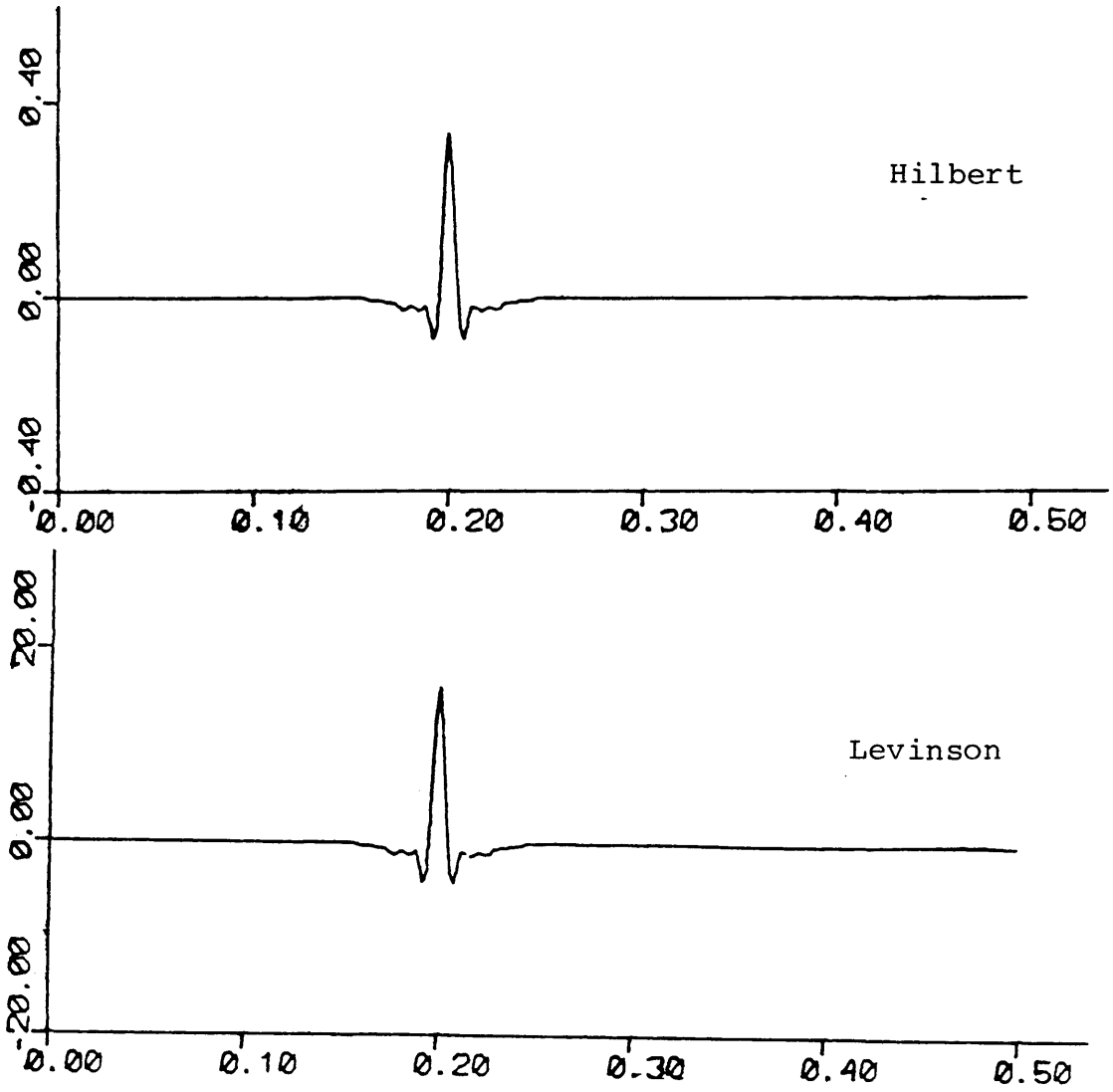

Figure 2B. Deconvolved wavelets of the Aquapulse source

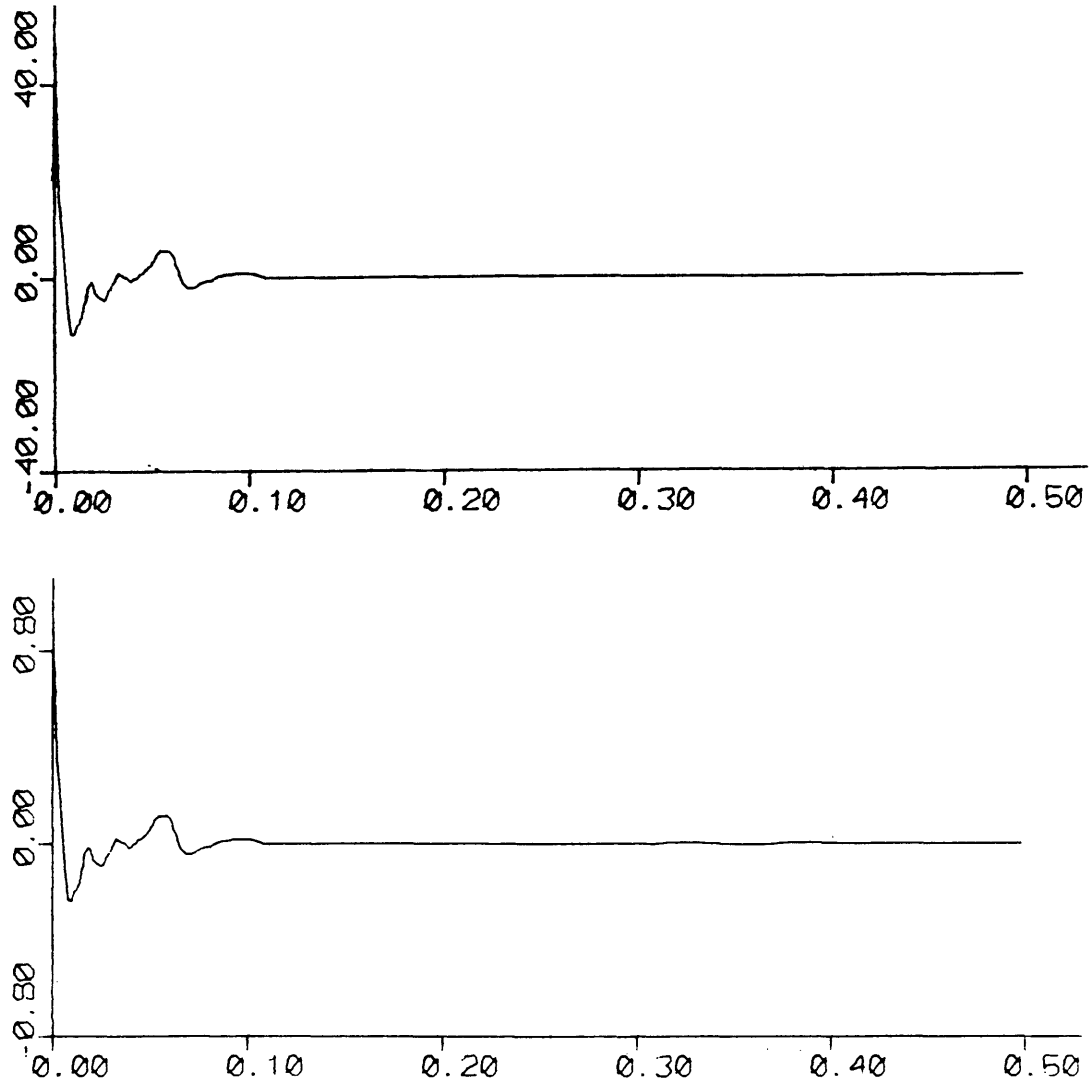

Figure 2C, Estimates of the Aquapulse source

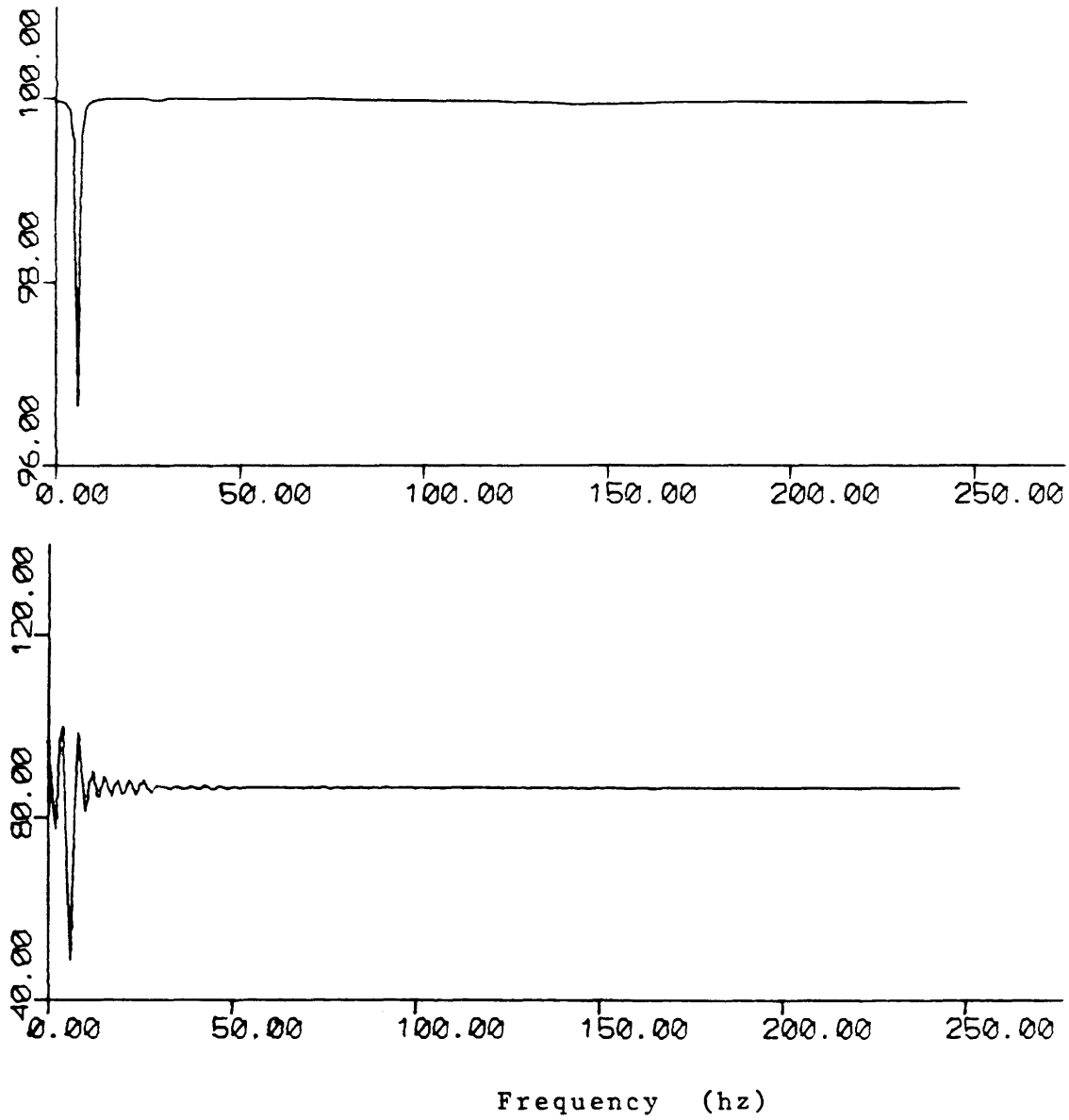

Figure 2D. Deconvolved amplitude spectra of the Aquapulse source.

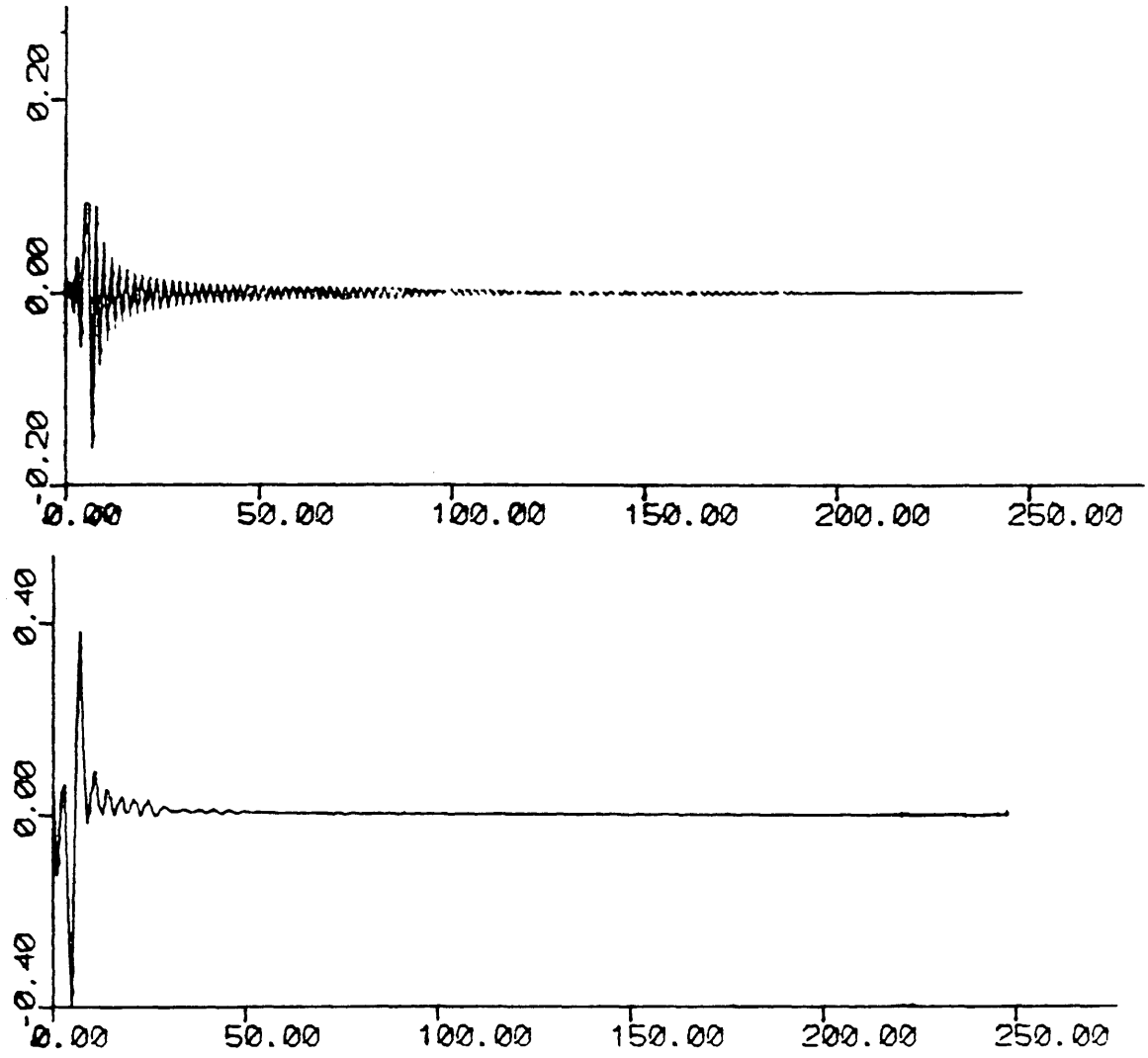

Figure 2E. Deconvolved phase spectra of the Aquapulse source.

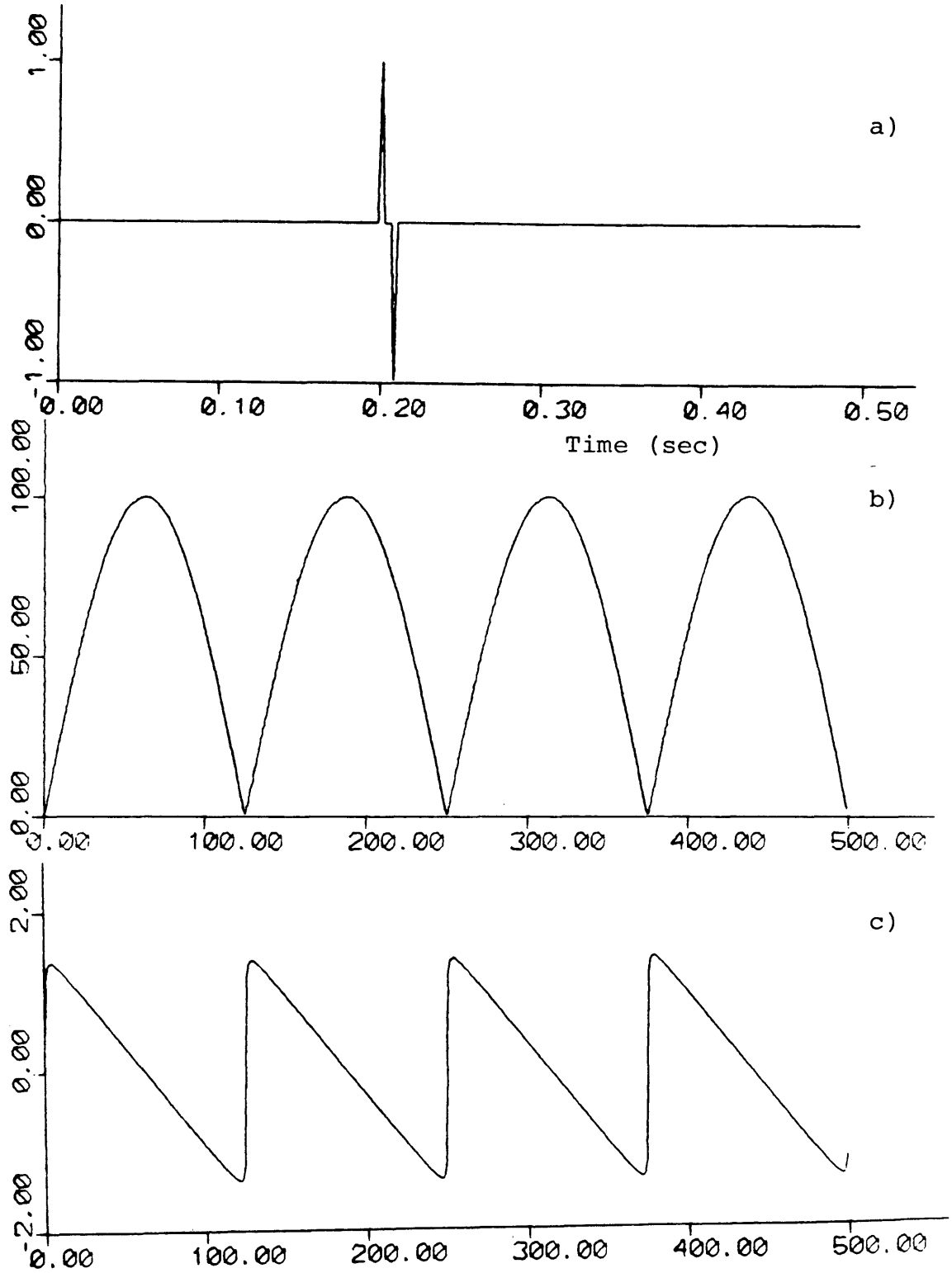

Figure 3A. Ghosting filter. a) Impulse response. b) Amplitude spectrum. c) phase spectrum.

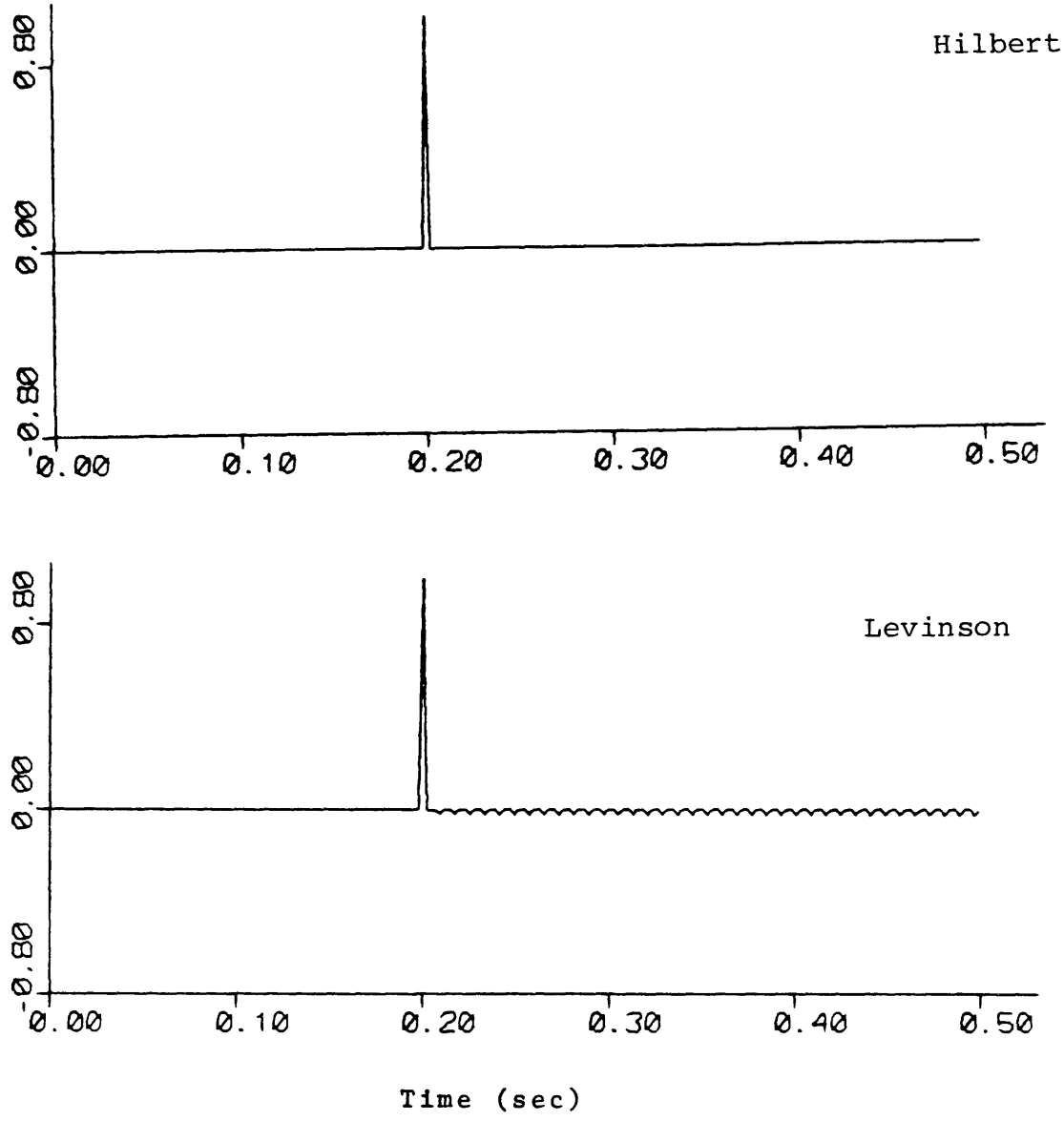

Figure 3B. Deconvolved wavelets of the ghosting filter.

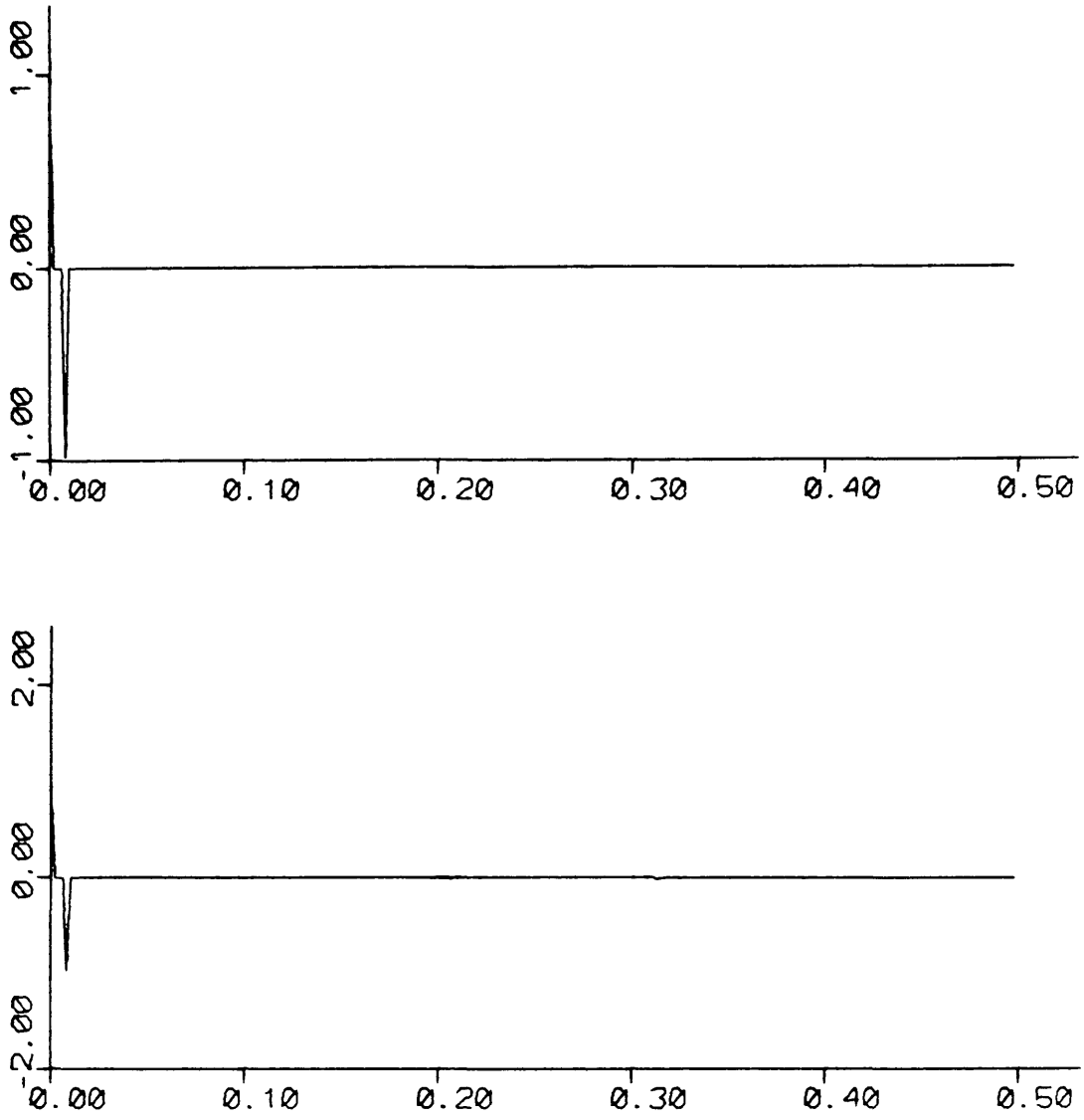

Figure 3C. Estimates of the ghosting filter.

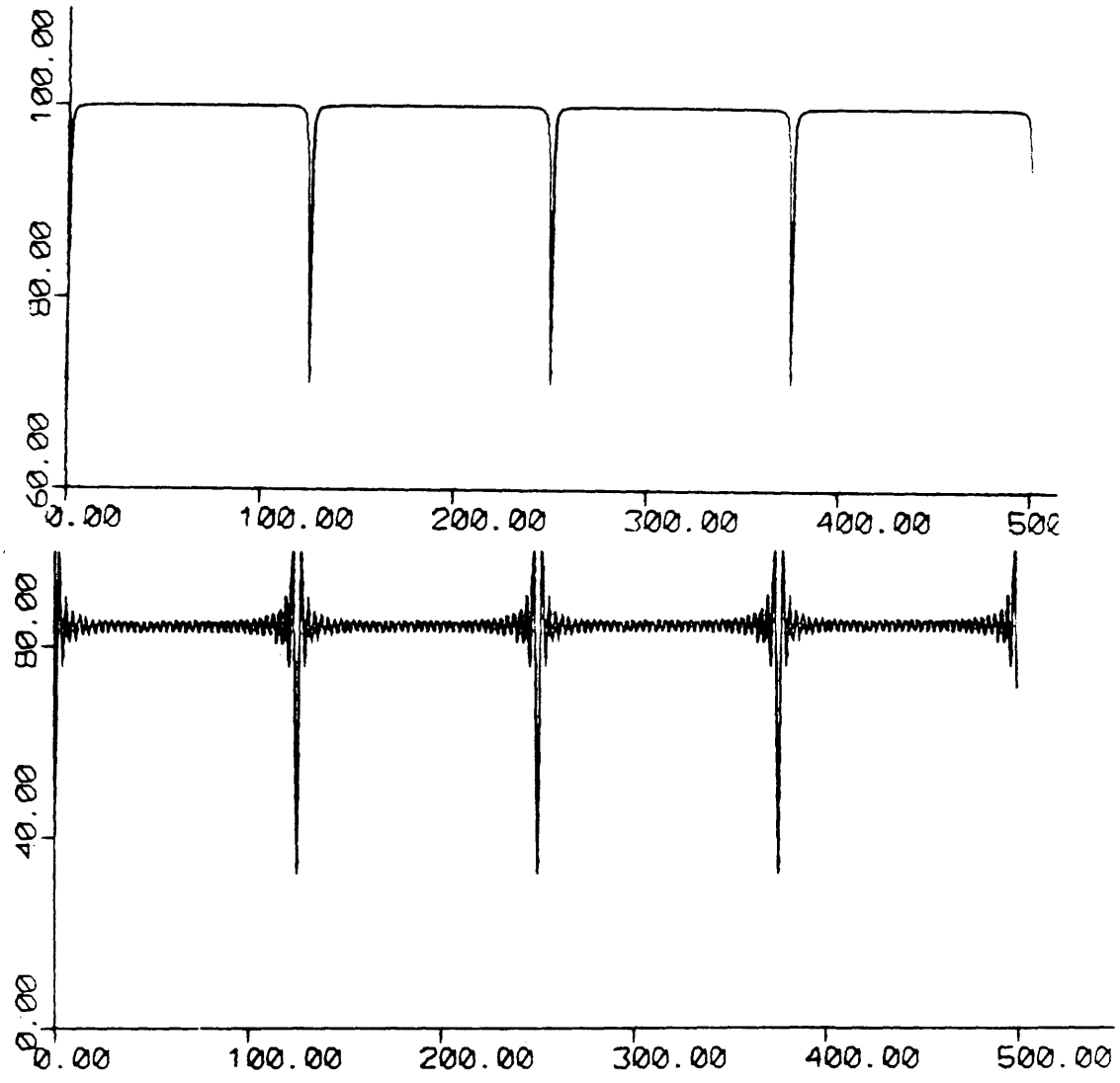

Figure 3D. Deconvolved amplitude spectra of the ghosting filter.

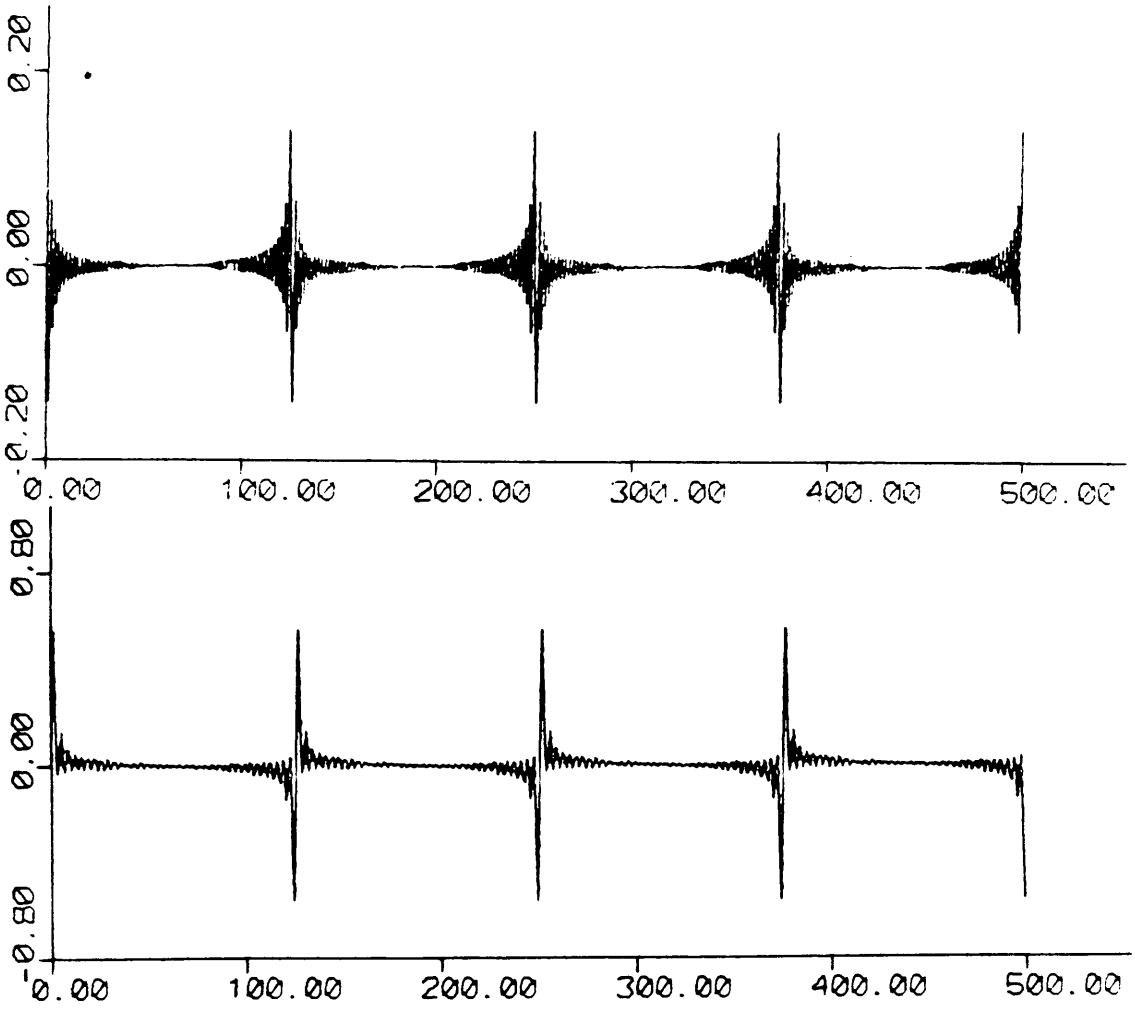

Figure 3E. Deconvolved phase spectra of the ghosting filter.

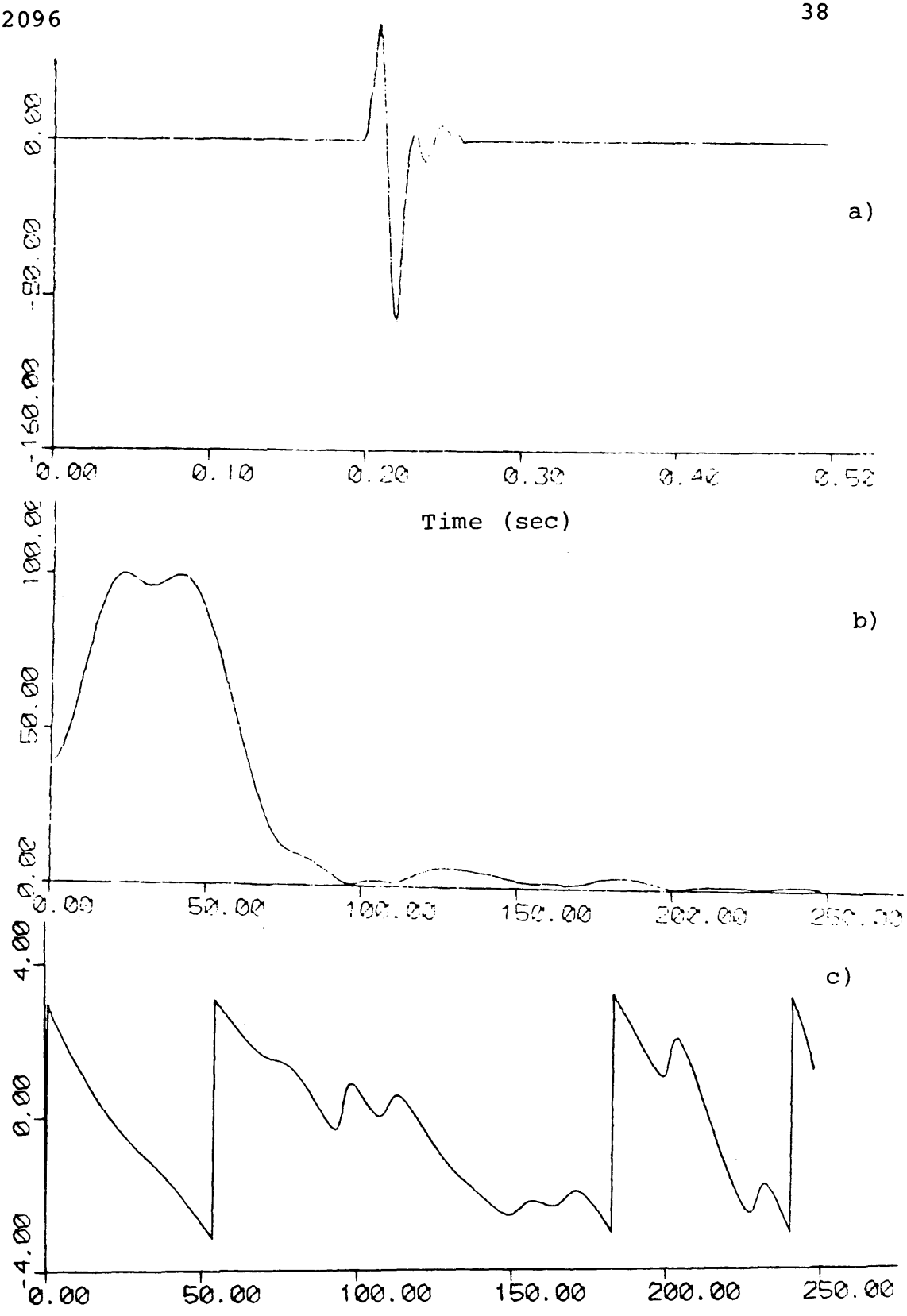

Figure 4A. Recording filter (8/18-62 hz). a) Impulse response. b) Amplitude spectrum. c) Phase spectrum.

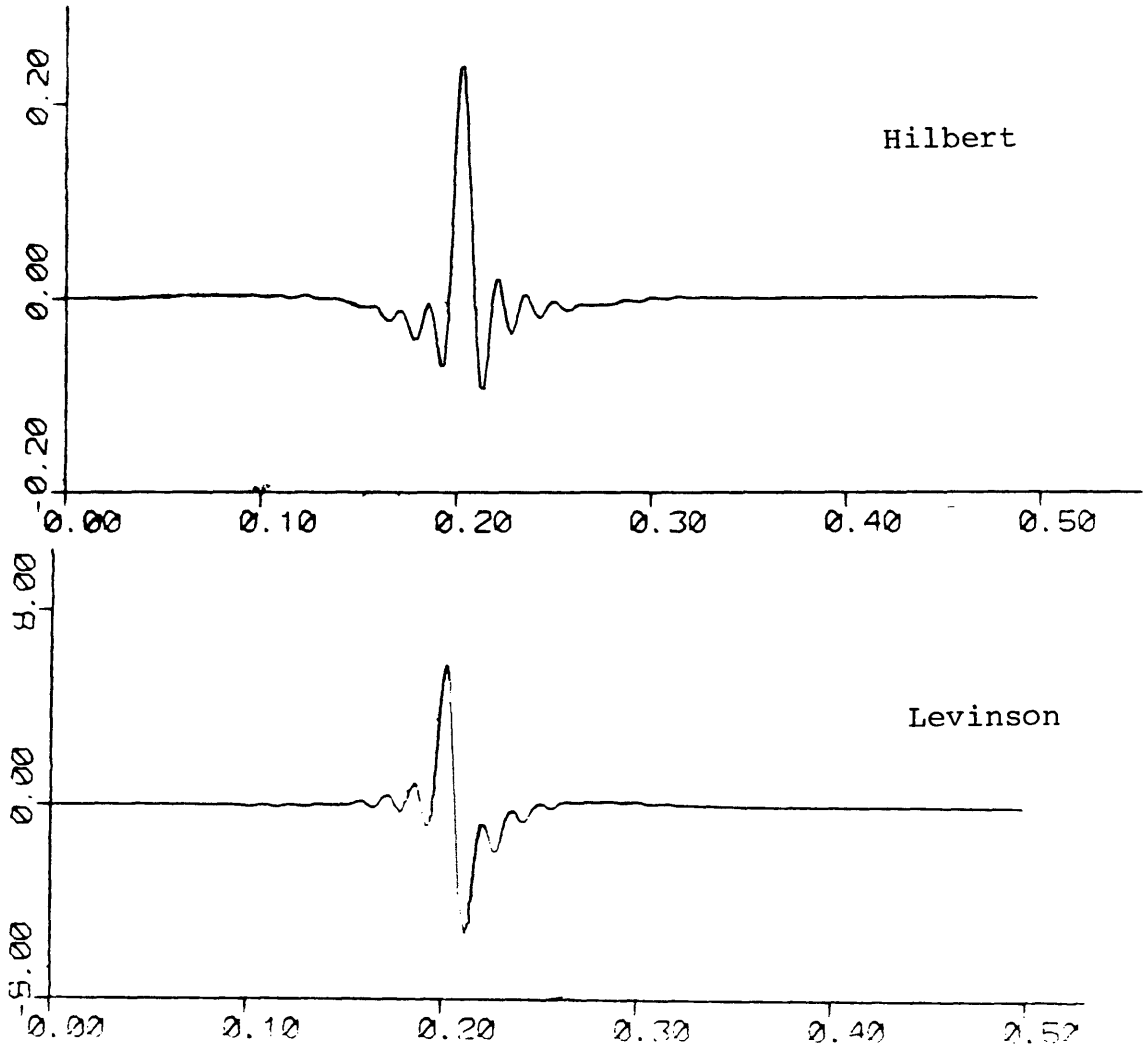

Figure 4B. Deconvolved wavelets of the recording filter.

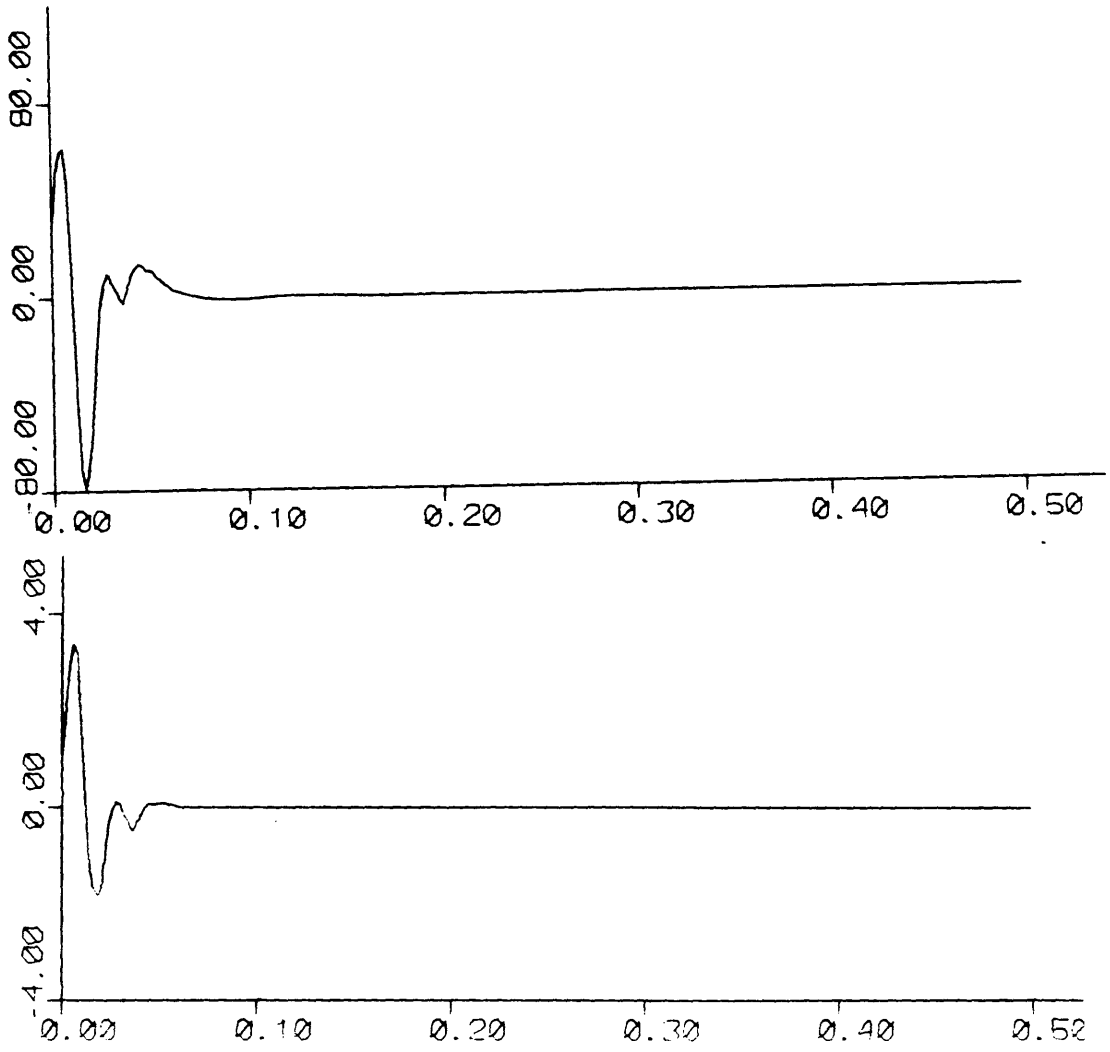

Figure 4C. Estimates of the recording filter.

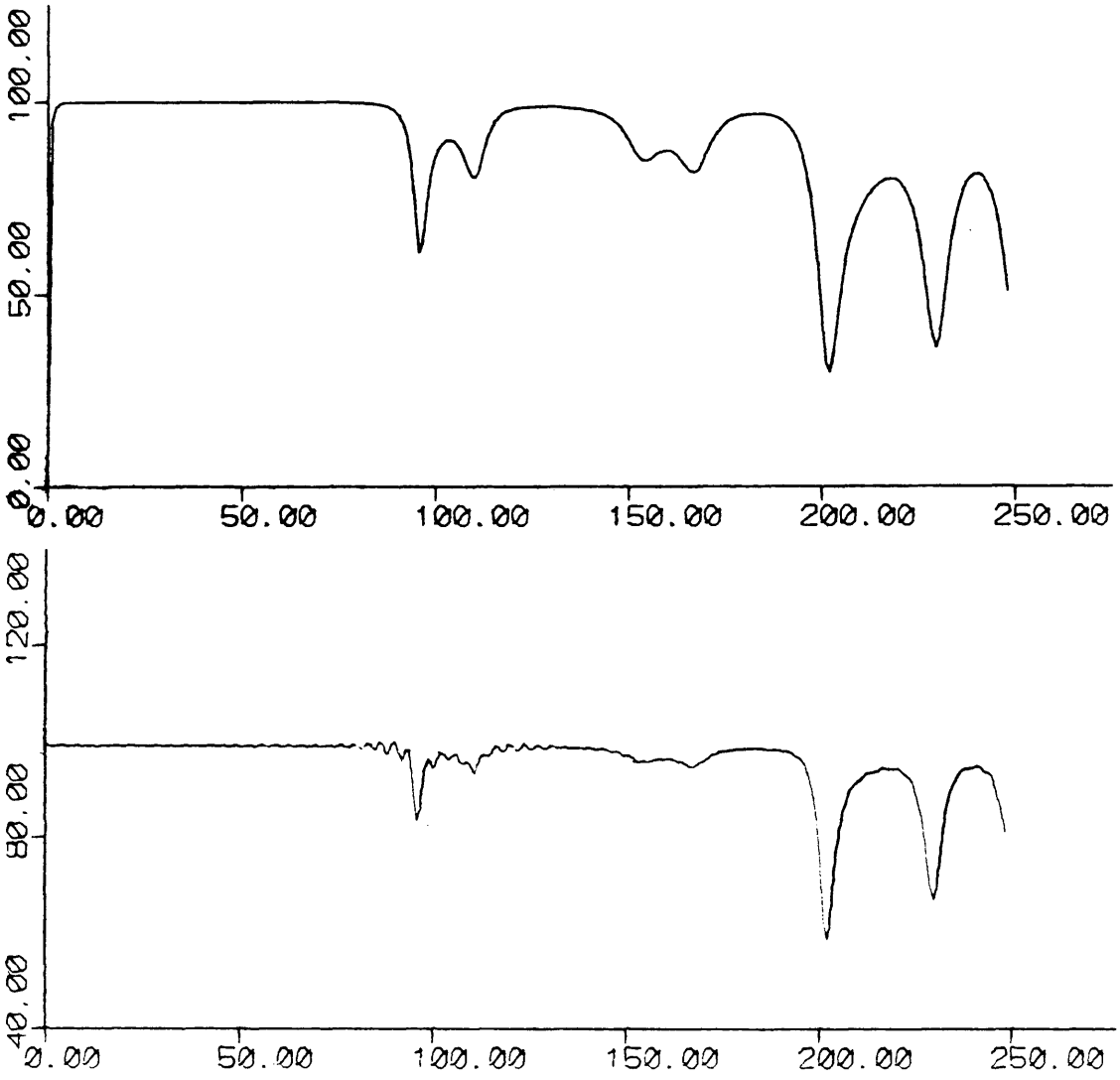

Figure 4D. Deconvolved amplitude spectra of the recording filter.

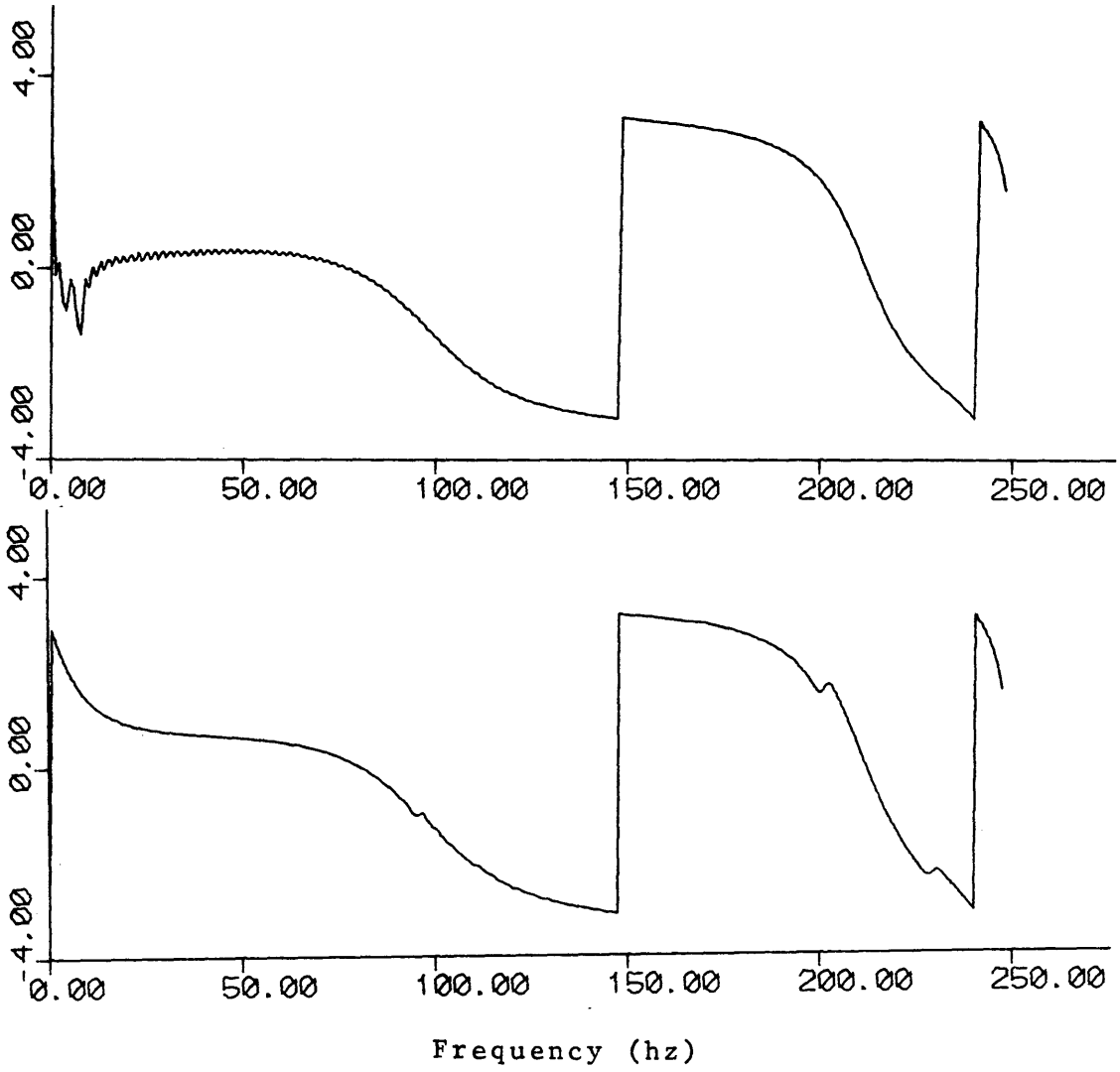

Figure 4E. Deconvolved phase spectra of the recording filter.

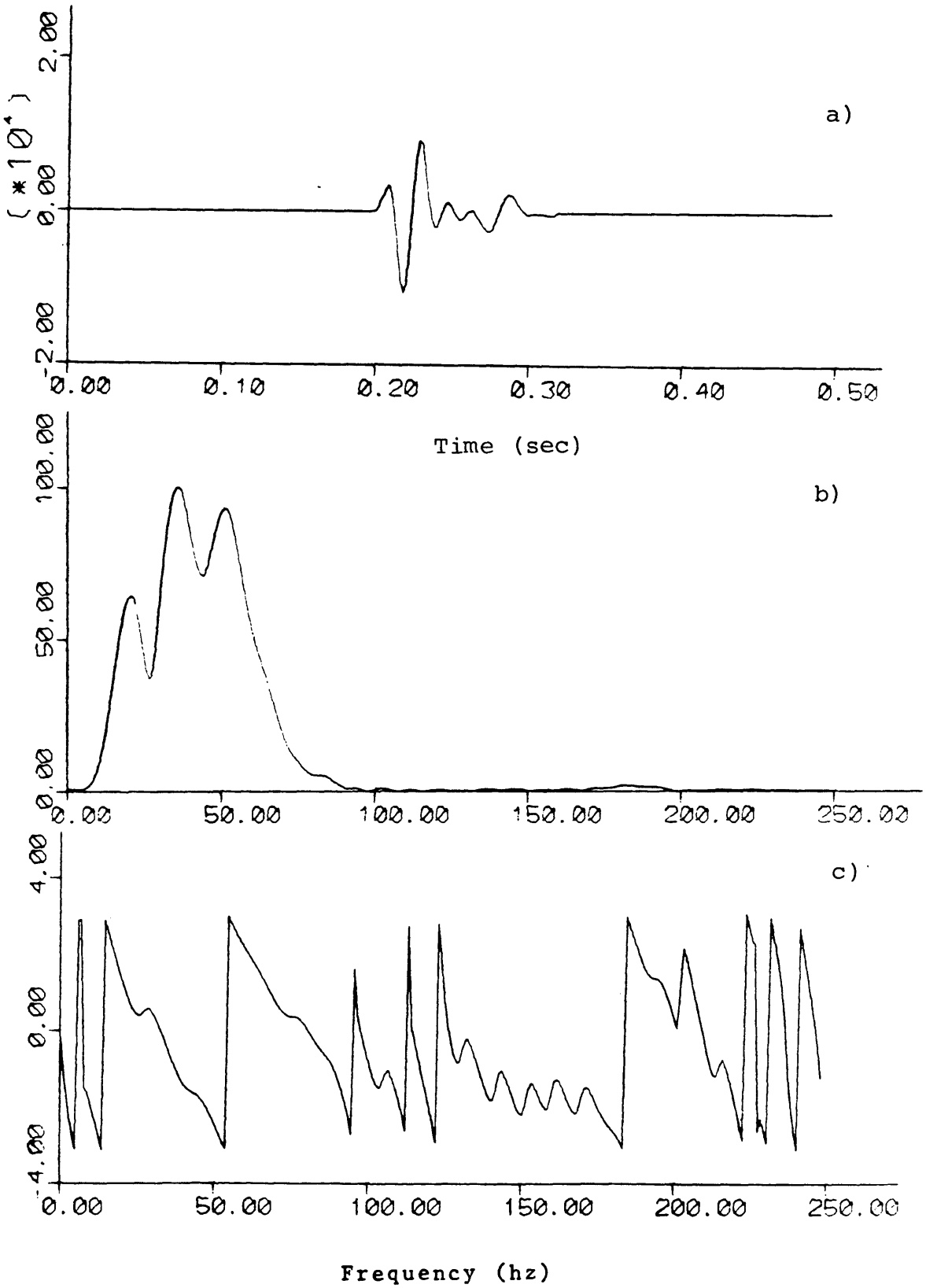

Figure 5A. The convolution of Aquapulse signature, ghost and recording filters. a) Impulse response. b) Amplitude spectrum. c) Phase spectrum.

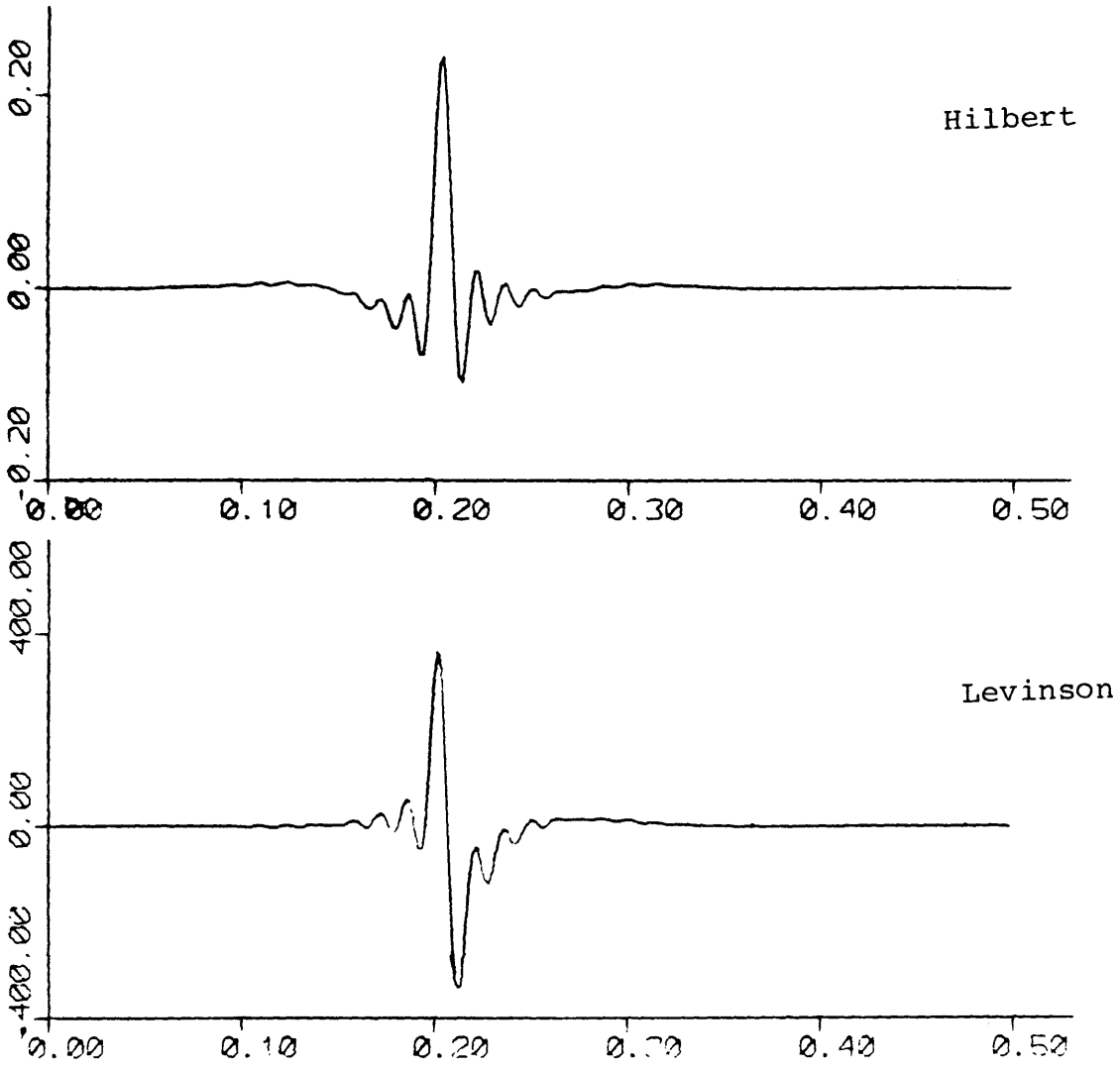

Figure 5B. Deconvolved wavelets of the composite system.

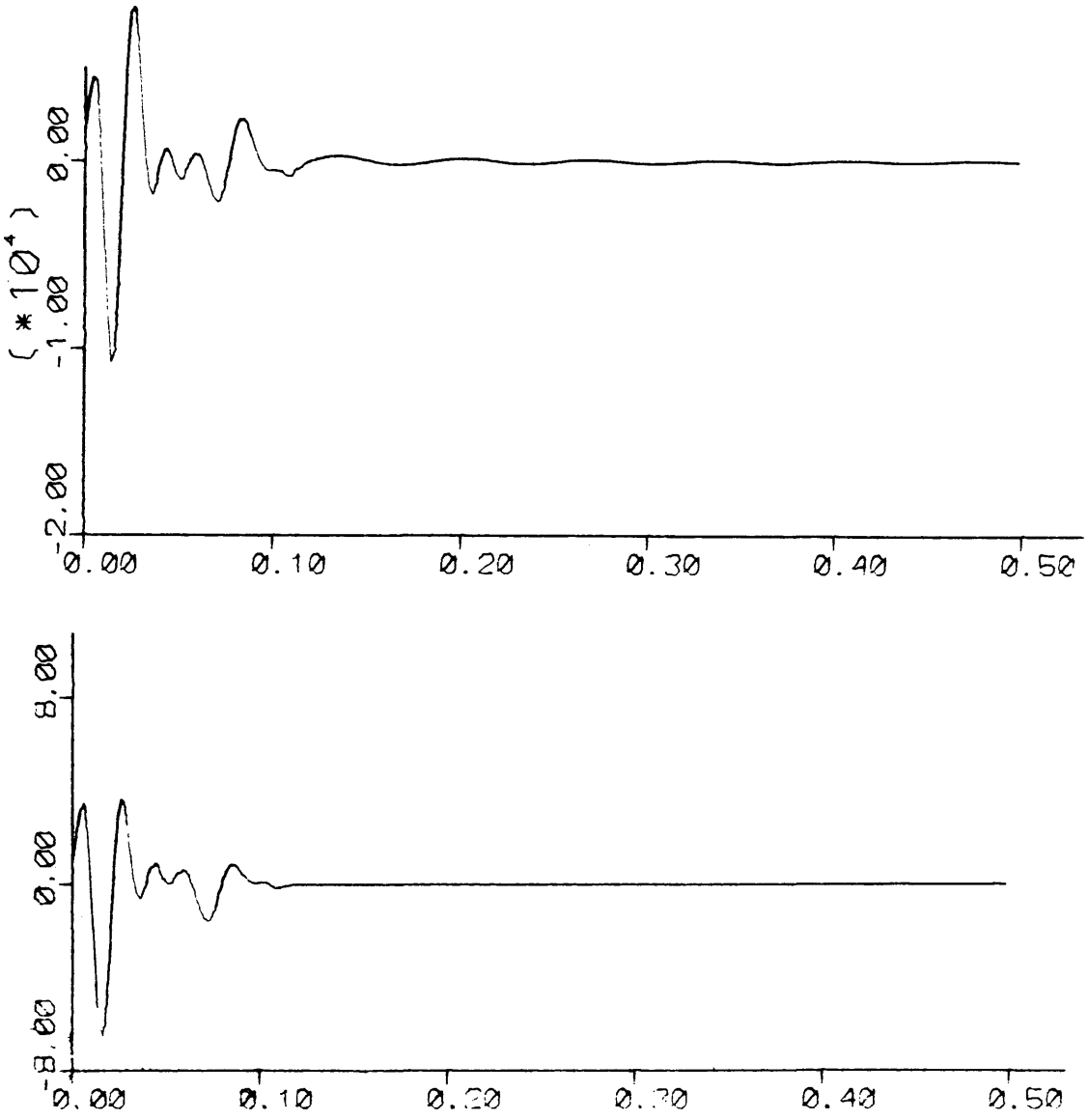

Figure 5C. Estimates of the impulse response of the composite system.

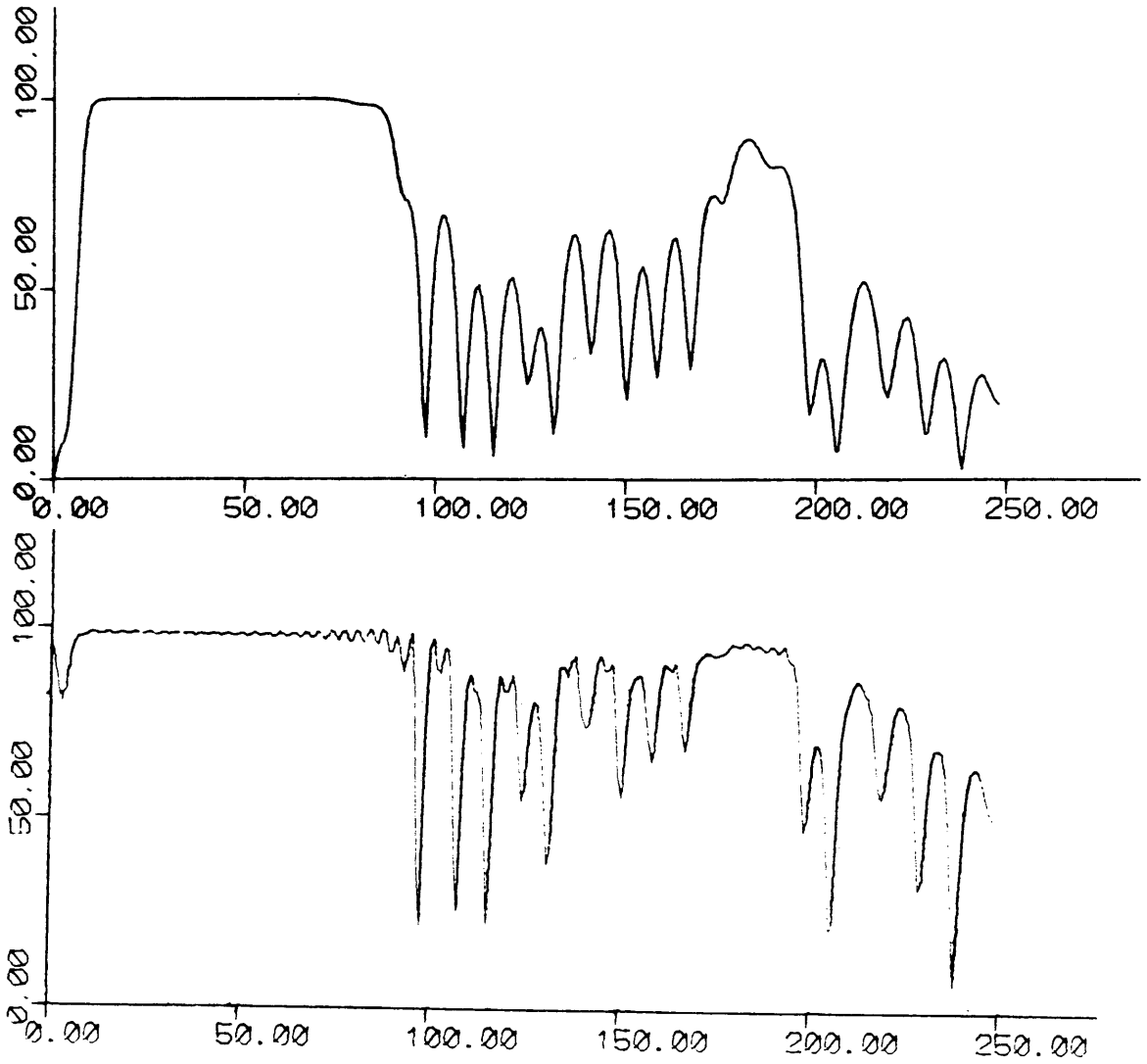

Figure 5D. Deconvolved amplitude spectra of the composite system.

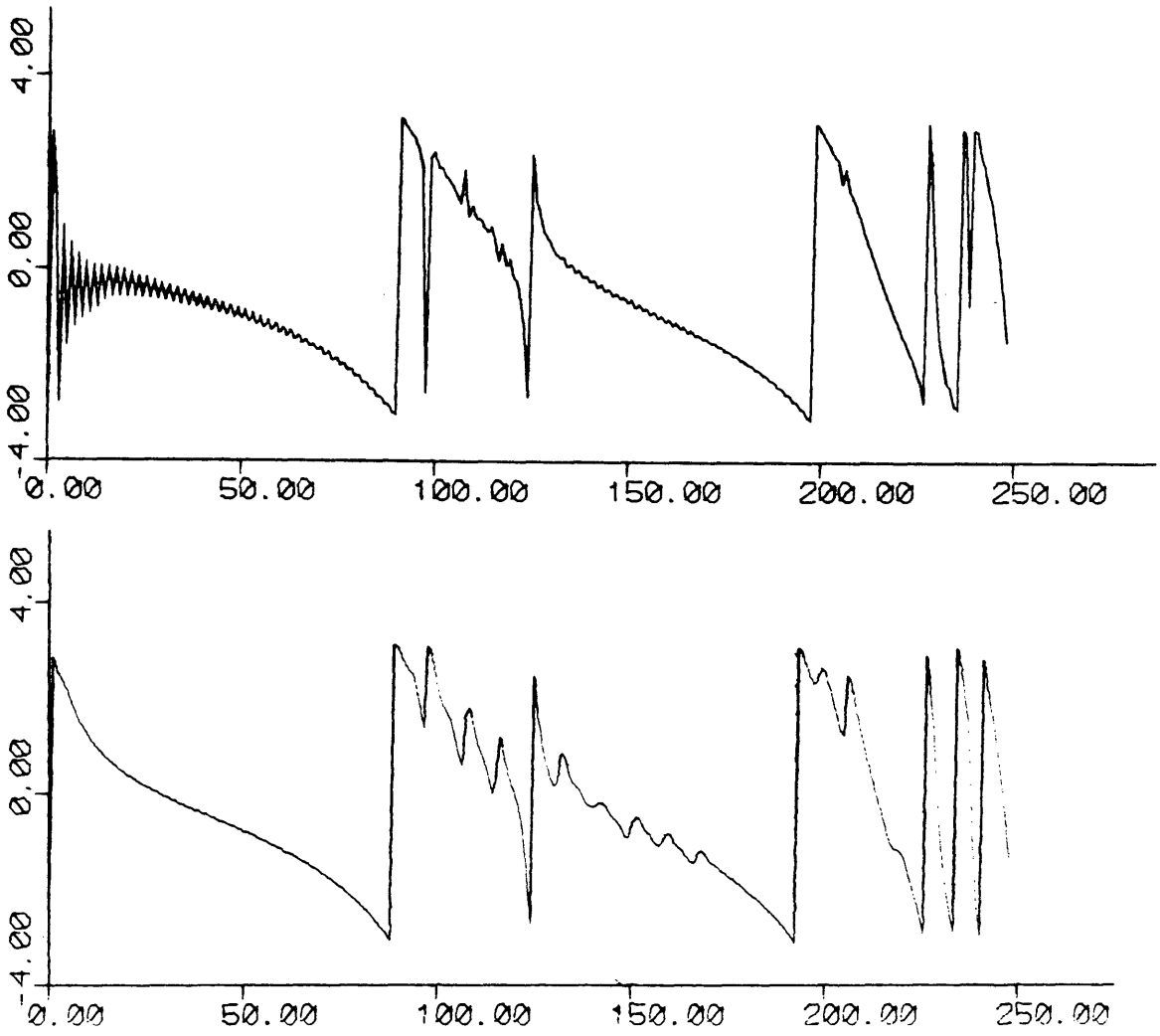

Figure 5E. Deconvolved phase spectra of the composite system.

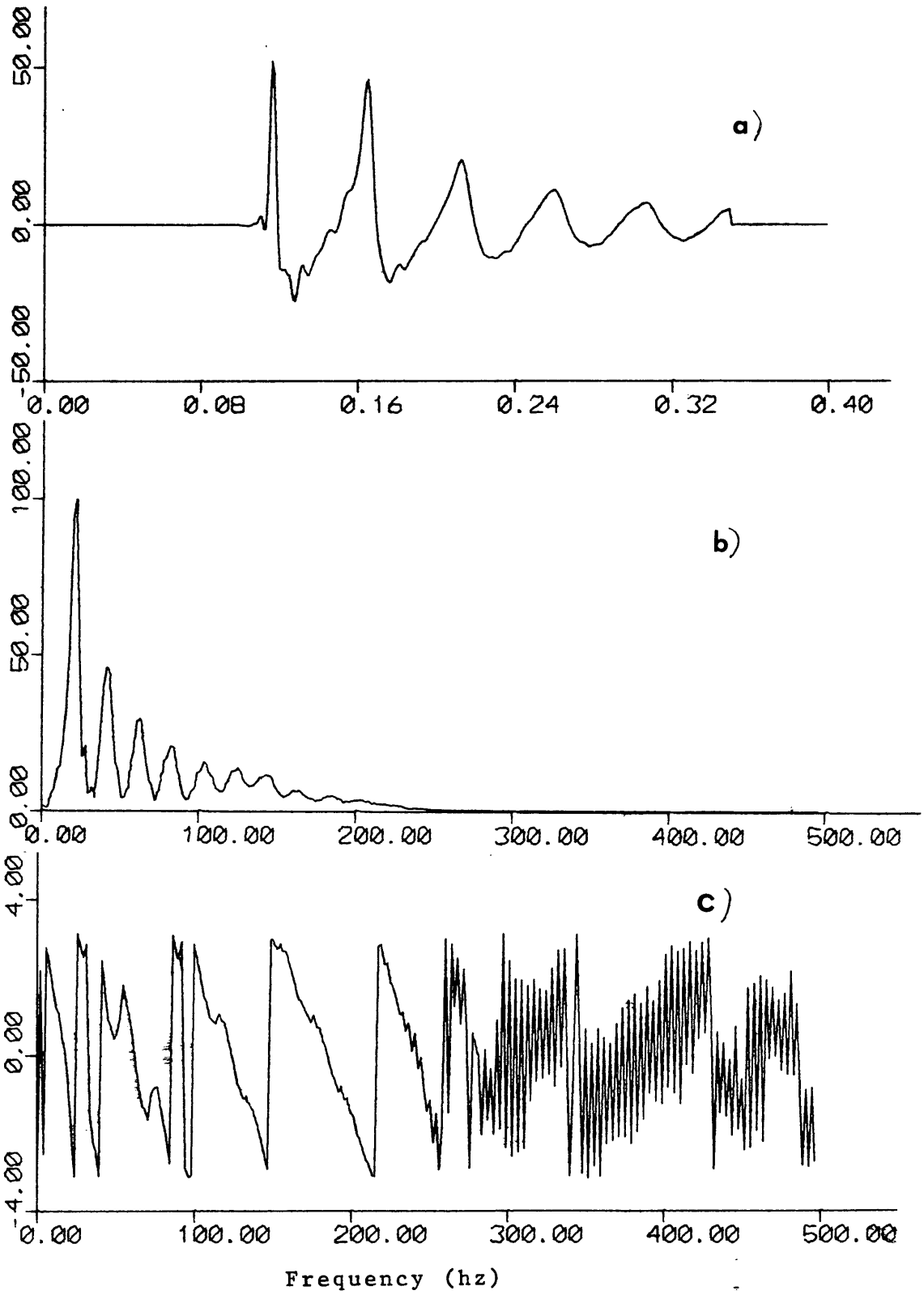

Figure 6A. 20 cu. in. airgun signature. a) Impulse response. b) Amplitude spectrum. c) phase spectrum.

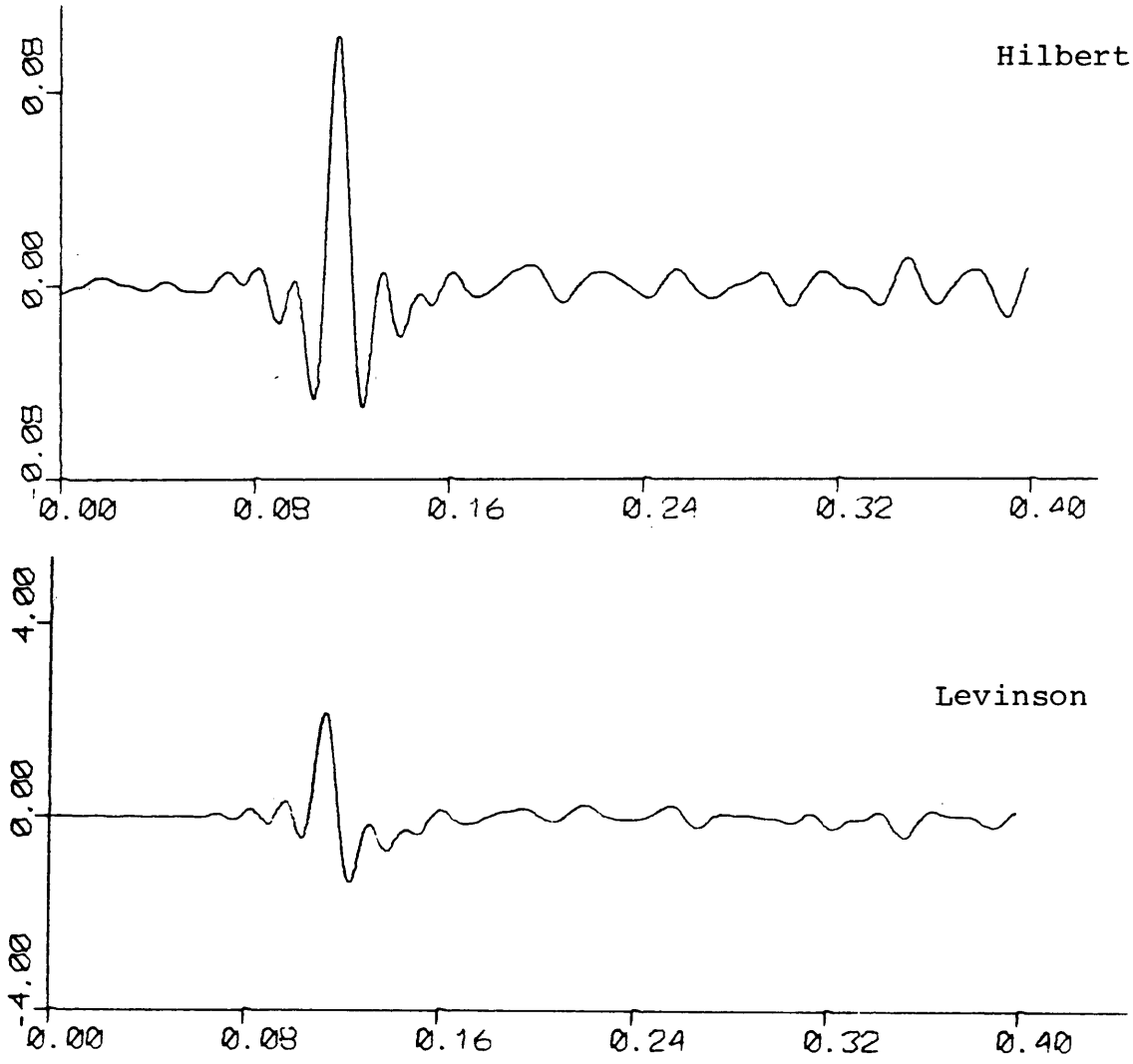

Figure 6B. Deconvolved wavelets of the 20 cu. in. airgun signature.

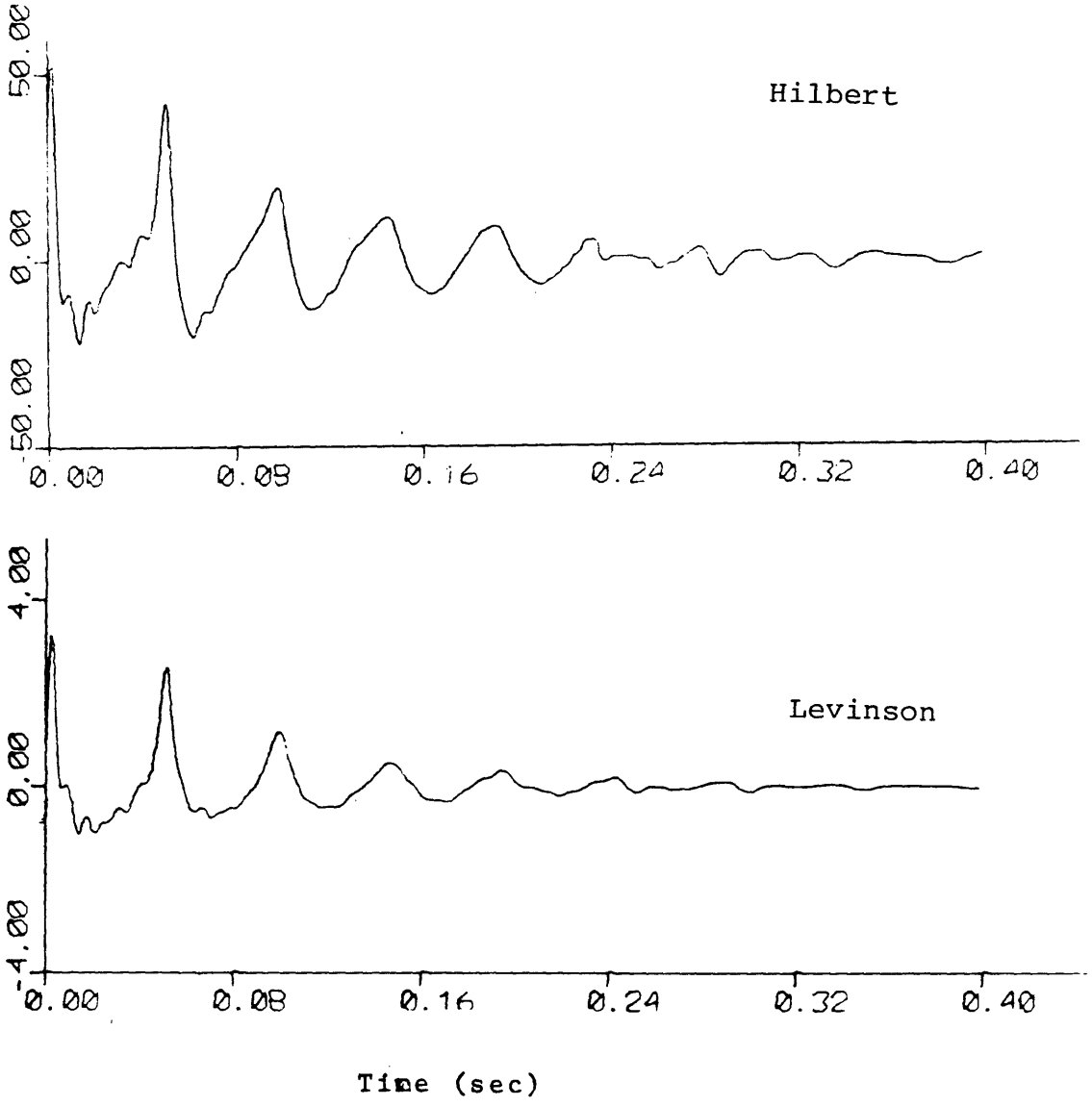

Figure 6C. Estimates of the 20 cu. in. airgun signature.

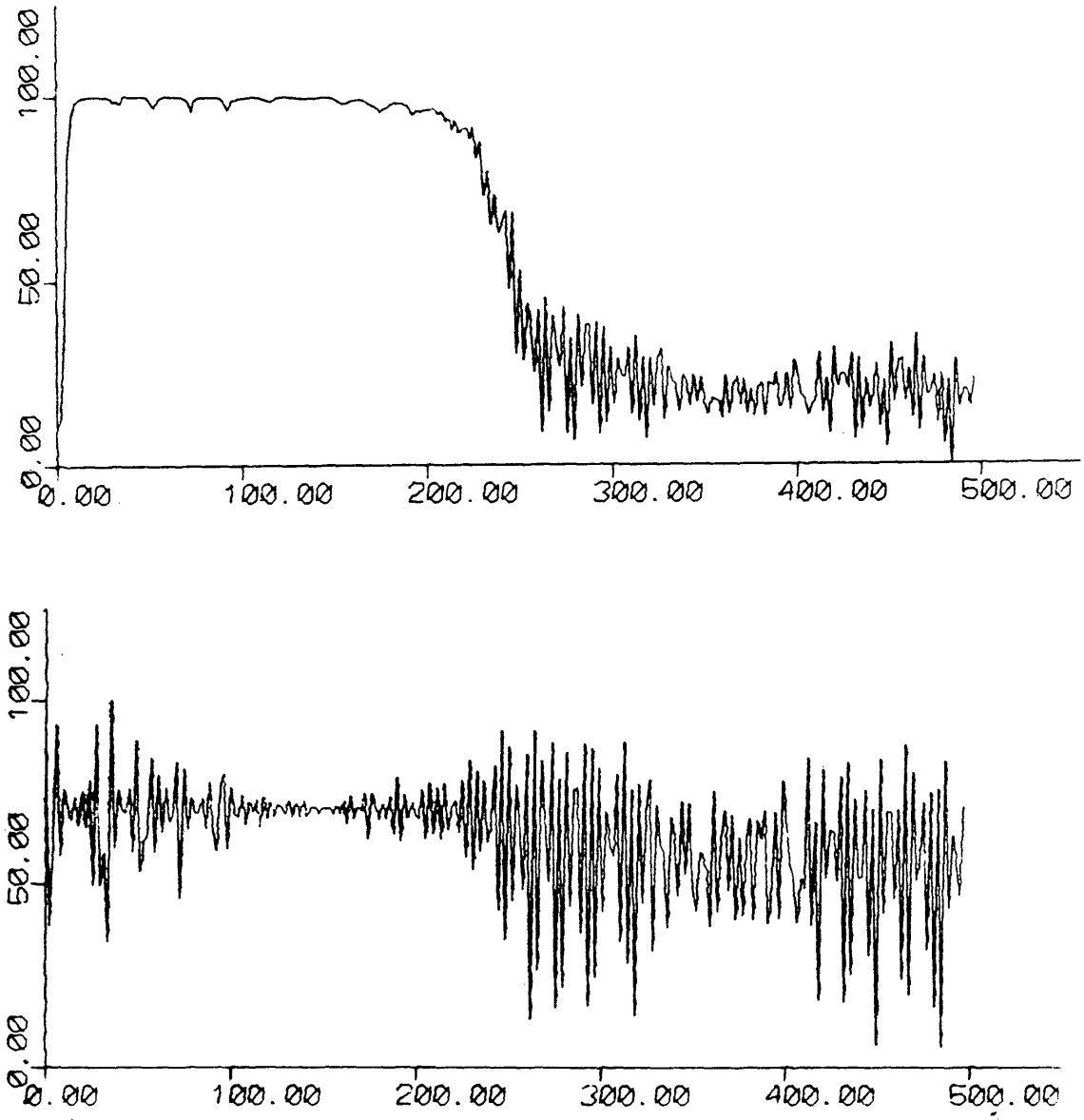

Figure 6D. Deconvolved amplitude spectra of the 20 cu. in. airgun signature.

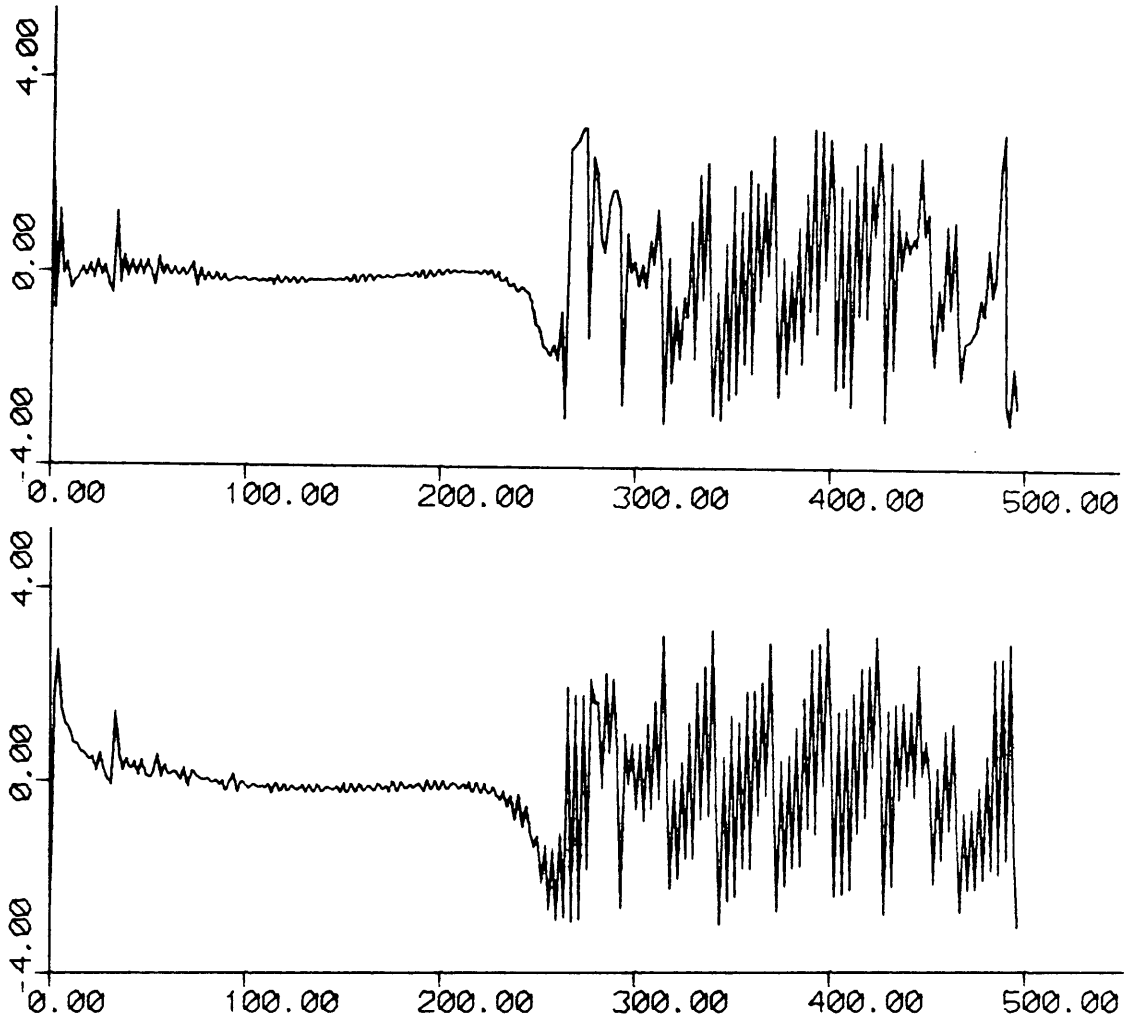

Figure 6E. Deconvolved phase spectra of the 20 cu. in. airgun signature.

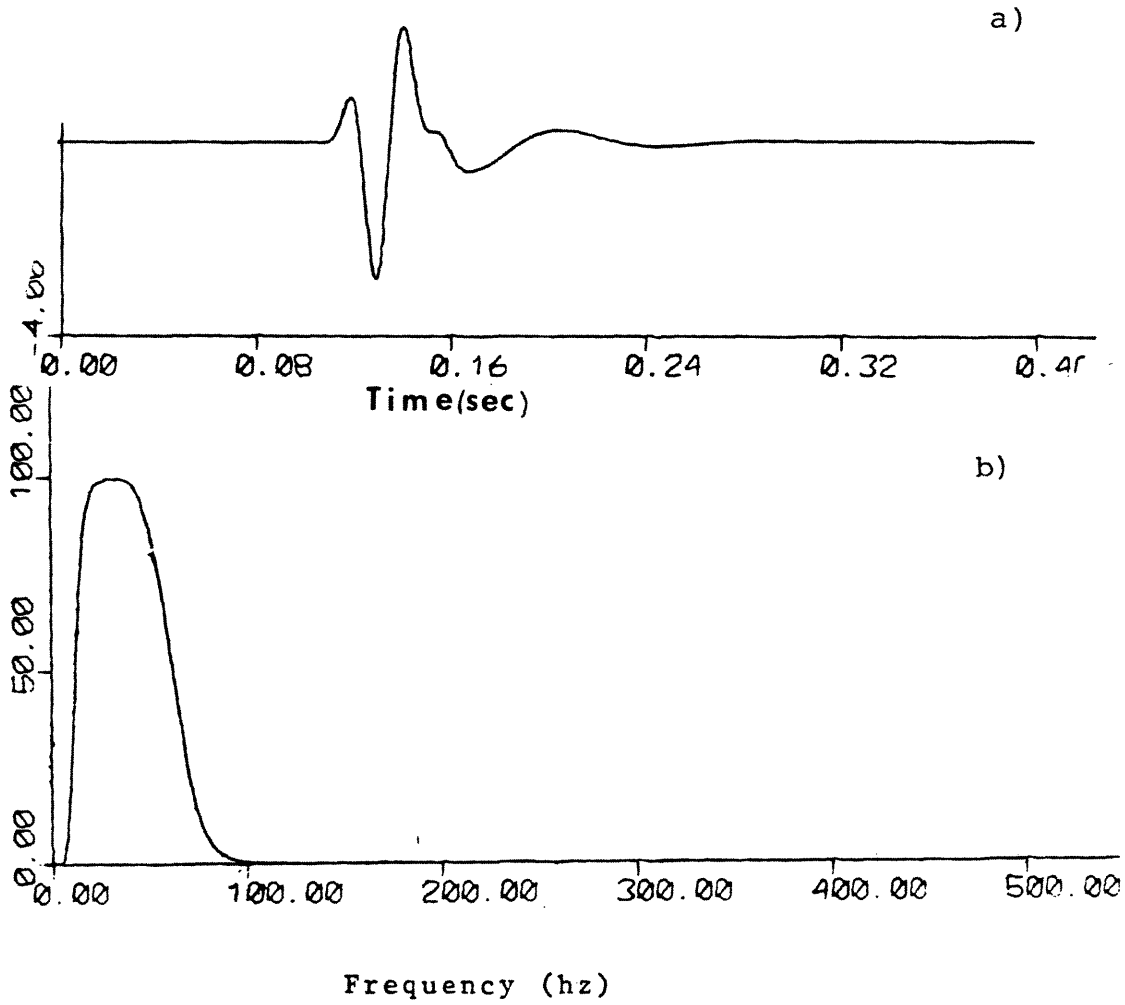

Figure 7A. a) Recording filter (8/36-62 hz) and b) Amplitude spectrum.

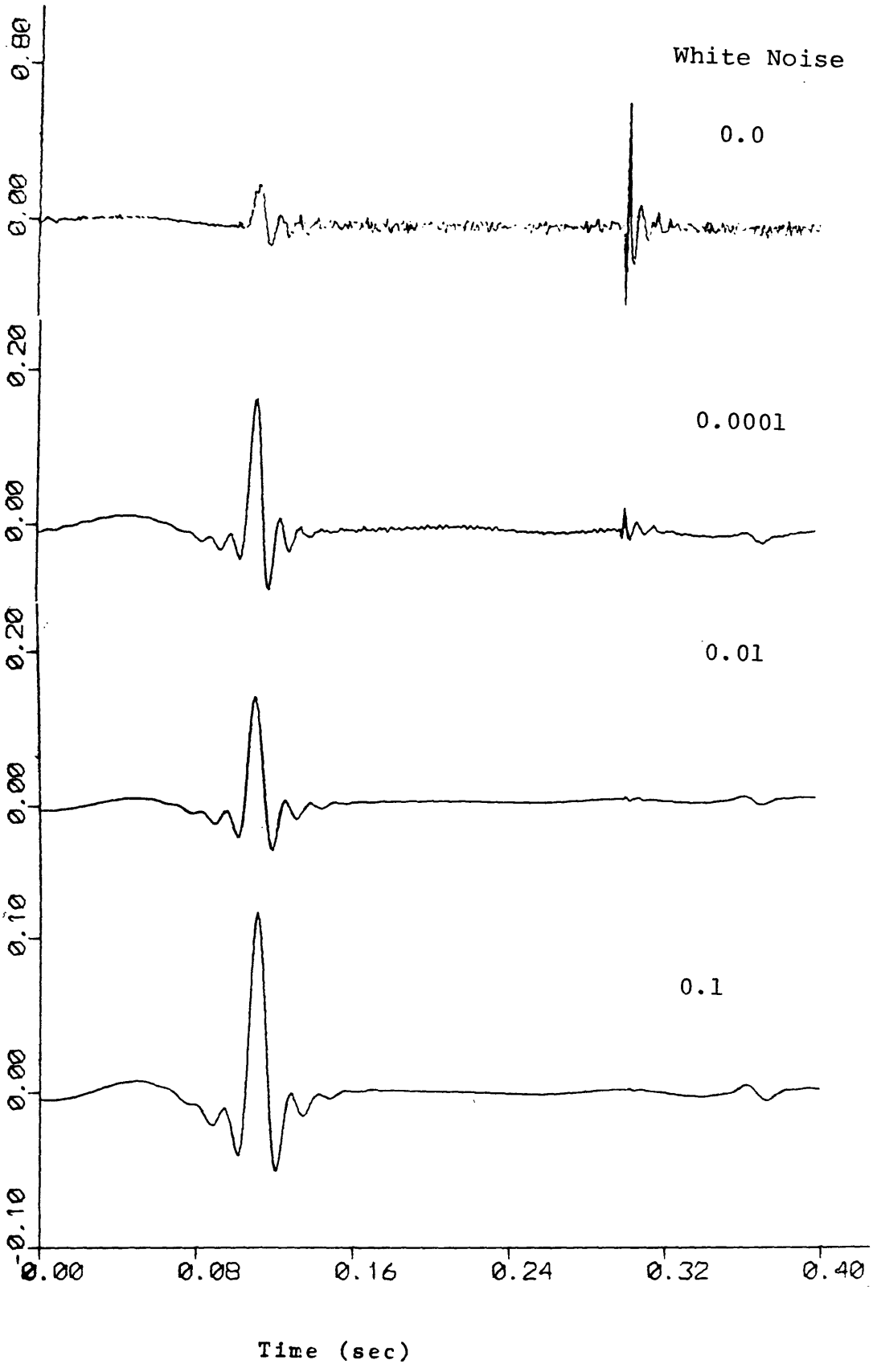

Figure 7B. Deconvolved wavelets of the recording filter in Figure 7A, with four different white noise levels, without band-pass filter, by the Hilbert transform.

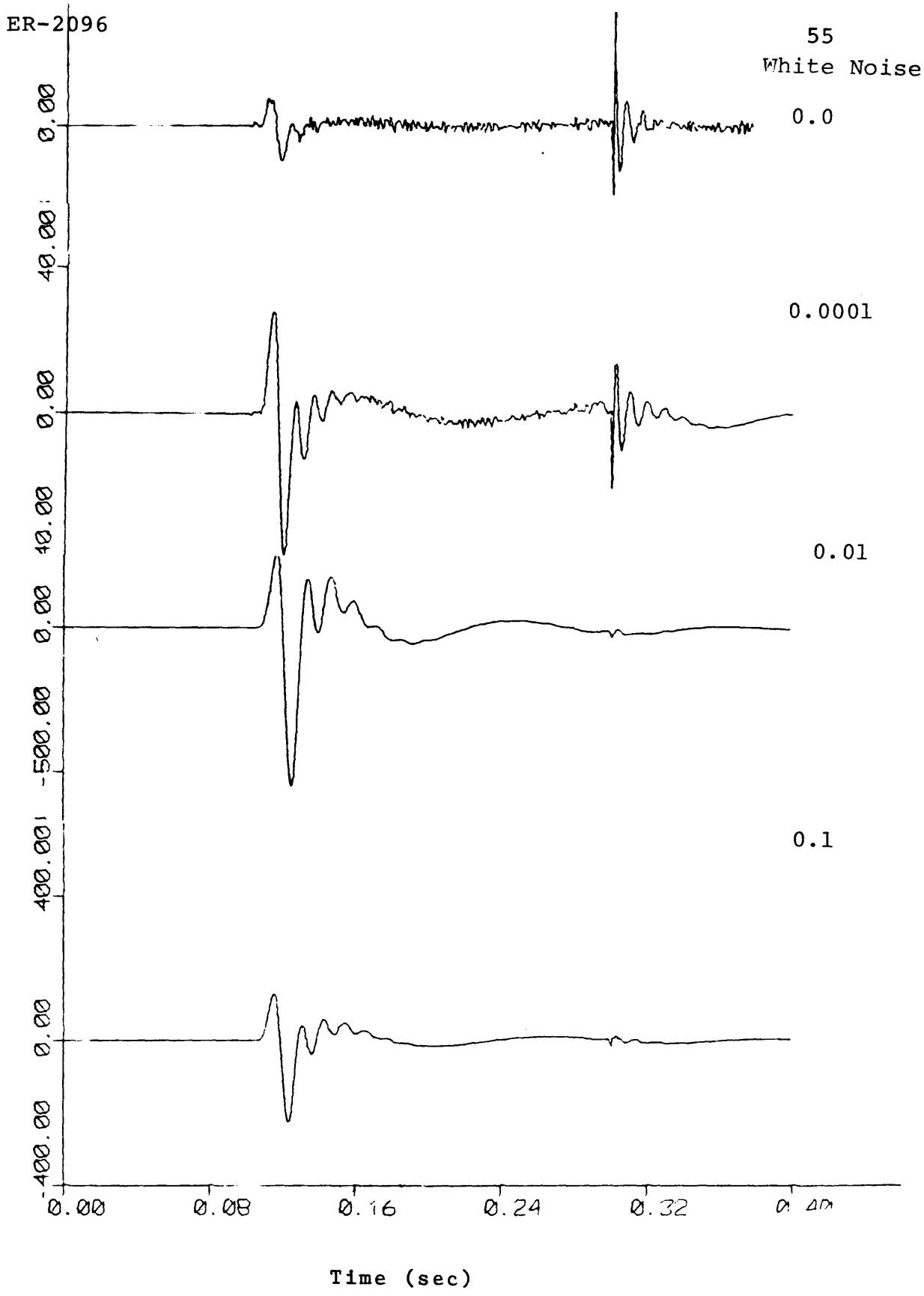

Figure 7C. Deconvolved wavelets of the recording filter in Figure 7A, with four different white noise levels, without band-pass filter, by the Levinson's algorithm.

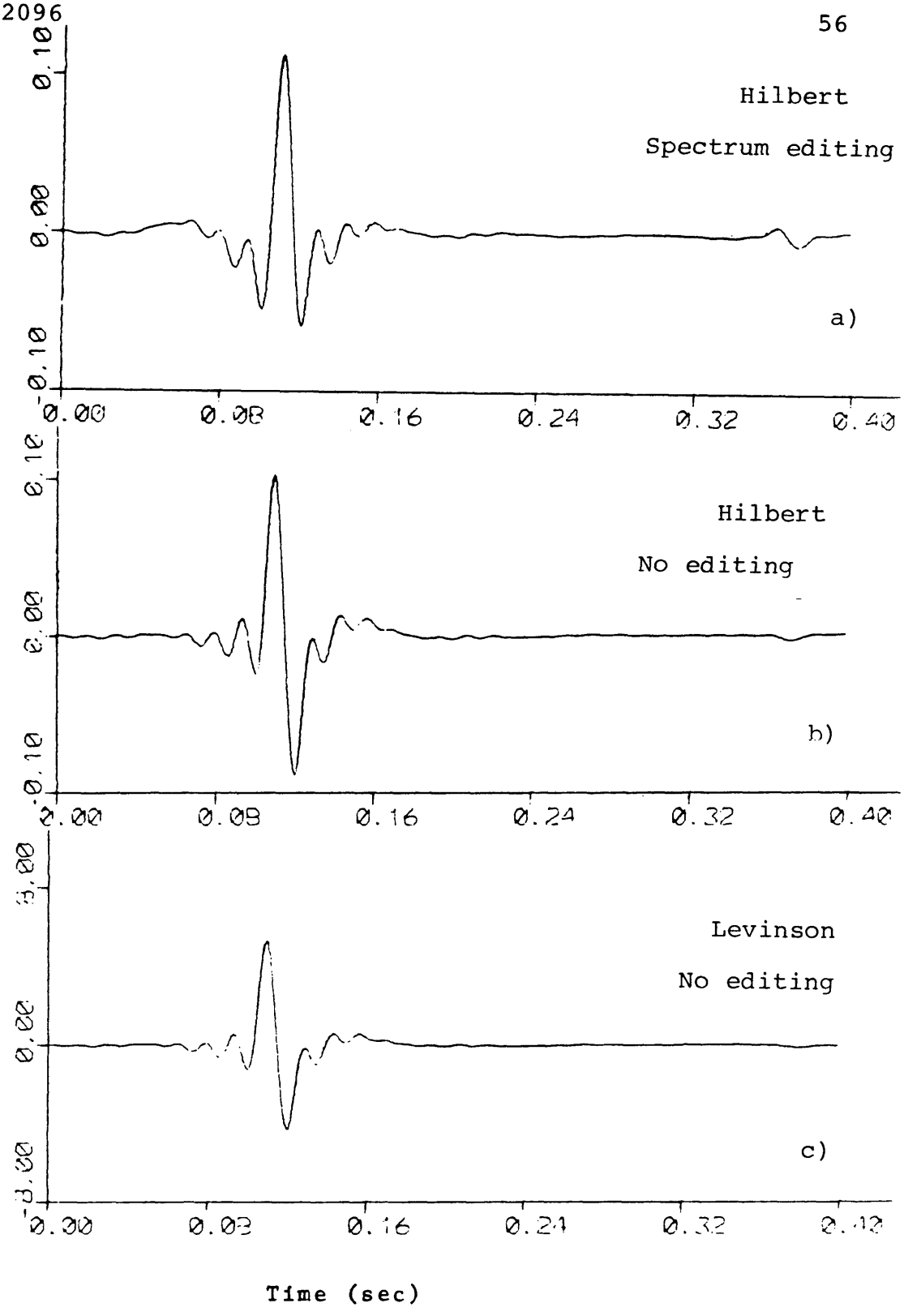

Figure 7D. Deconvolved wavelets of the recording filter in Figure 7A, With band-pass filter, white noise zero, a) & b) by the Hilbert transform, c) by the Levinson's method.

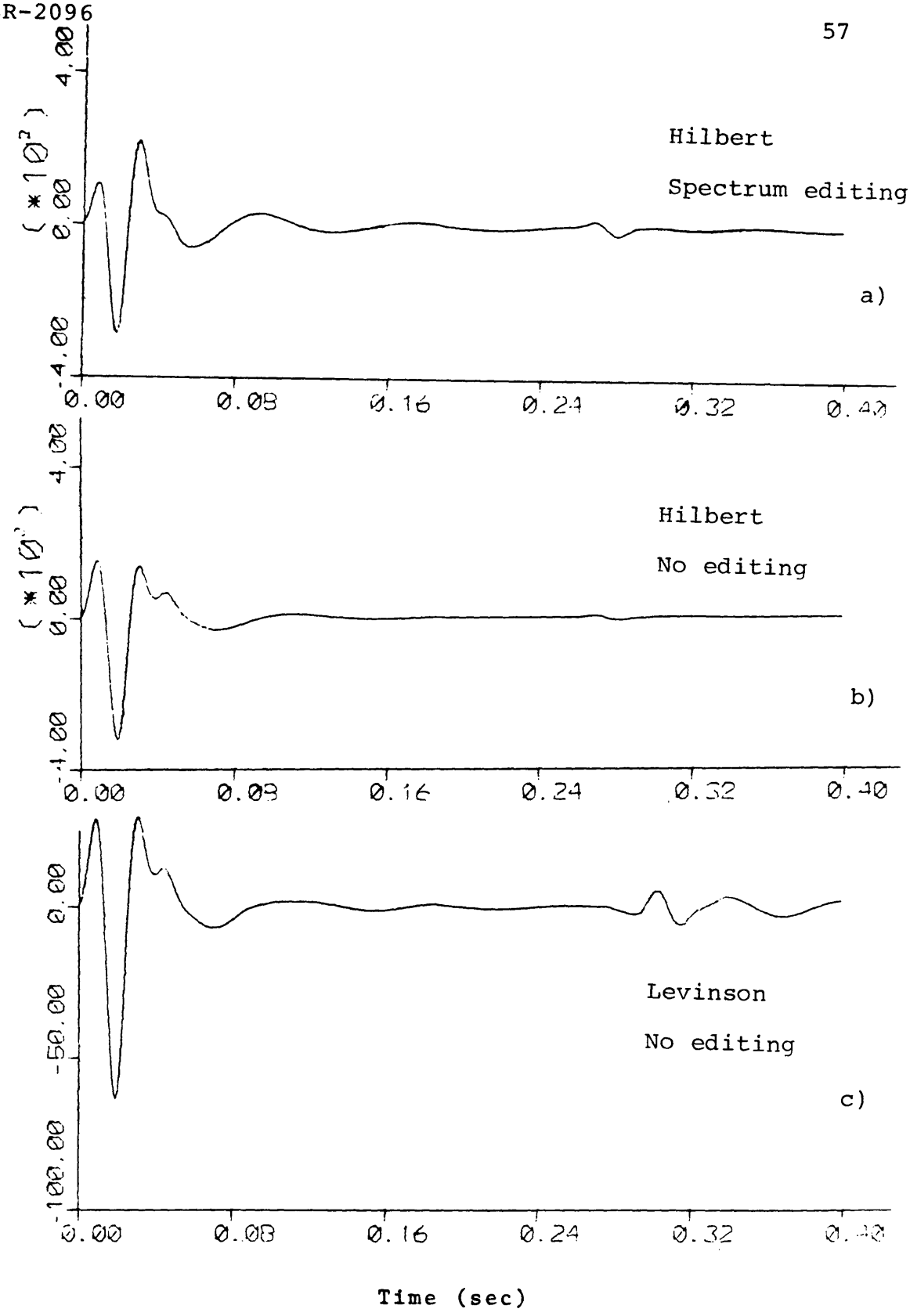

Figure 7E. Estimates of the recording filter in Figure 7A, white noise zero. a) & b) by the Hilbert transform, c) by the Levinson's method.

Part B. Receiver Array Response

In this part we deal with those arrays which involve, like most geophone group cables, a simple addition of the outputs of the detectors.

The time delay ΔT across an array of length ΔX for a plane wave is given by

$$\Delta T = \Delta X/c = (M-1)\Delta L/c, \qquad (13)$$

where c is the phase velocity, M is the number of detectors, and ΔL is the detector spacing. ΔT can be called the duration of the array response.

Consider discrete array response a(t) with duration of ΔT, we could have

$$a(t)=\begin{cases}\sum_{n=-N}^{N}\delta(t-n\Delta\tau), & \text{for } 2N\Delta\tau = \Delta T,\ M = 2N+1\\ \sum_{n=-N}^{N-1}\delta(t\pm n\Delta\tau), & \text{for } (2N-1)\Delta\tau=\Delta T,\ M = 2N.\end{cases} \qquad (14)$$

Here, we use $\Delta\tau = \Delta L/c$ as the time interval between elements of the array.

The Fourier transform of a(t) would be

$$A(f)=\begin{cases}\left|\frac{1}{2N+1} + \frac{2}{2N+1}\sum_{l=1}^{N}\cos(2l\pi f\Delta\tau)\right| \exp(jp)\\ \left|\frac{1}{N}\sum_{l=1}^{N}\cos[(2l-1)\pi f\Delta\tau]\right| \exp j[\pm\pi f\Delta\tau+p]\end{cases} \qquad (15)$$

where $\pm\pi f\Delta\tau$ is the phase shift due to non-symmetric sampling of $\Delta\tau/2$ for the even-number elements (M=2N), and $p=\pi/2$ sgn (A(f)) - $\pi/2$.

Equations (13) and (15) show that increasing the array length ΔX, i.e., increasing the duration of the array response ΔT, and the number of detectors has two effects on frequency spectrum:

1. The width of the rejection band increases.
2. The amplitude spectrum in the rejection band decreases (Figures 8 and 9).

A question of interest in high resolution is, how much of the signal bandwidth outside the central pass-band of the array can be restored, i.e., can all the signal energy in the recording filter band be used effectively?

The effect of array response depends on its duration. Now, we may simulate three cases of array responses with three different numbers of elements and durations for ΔL(22 ft) and c(11,000 ft/sec).

	M	ΔT(ms)	
Case 1. $a_1(t)$	1,	$\simeq 0$	$a_1(0) = 1$
Case 2. $a_2(t)$	2,	2,	$a_2(-1) = 1/2$, $a_2(0)=1/2$
Case 3. $a_3(t)$	4,	6,	$a_3(-2) = 1/4$, $a_3(-1)=1/4$
			$a_3(0) = 1/4$, $a_3(1)=1/4$

$\Delta\tau$ = 2 ms

Here the study investigates what problems the receiver array responses cause for the two types of deconvolution processes under consideration.

In Case 1, the duration of the array response approaches zero, thus the response should be the delta, and its amplitude spectrum is a flat line. Figures 8 and 9 show the impulse responses and the amplitude spectra of the array filters in Case 2 and Case 3, respectively.

A simulated minimum-phase recording filter (Figure 10) was used to convolve with each array filter. The convolution of the recording filter with $a_1(t)$ is still the recording filter. Figure 11 shows the impulse response and the amplitude spectrum of the convolution between the recording filter and the array $a_2(t)$. Figure 12 shows the similar results for $a_3(t)$. Figures 13 to 16 show the deconvolved amplitude spectra, wavelets and phase distortions obtained in the frequency domain by applying the Hilbert transform and the zero-phase bandpass filters to the three input wavelets in Figures 10, 11, and 12. Figure 17 shows three minimum-phase Hilbert transform estimates of the three input wavelets. The deconvolved results from Case 1 to Case 3, are shown in each figure from the top to the bottom. Figures 18 to 21 show the similar results obtained in the

time domain by applying the one-sided least-squares deconvolution operators and the zero-phase bandpass filters to the above three inputs. Figure 22 shows three estimates of the above three inputs, obtained by inverting the one-sided least-squares operators computed from the autocorrelation functions of the input wavelets.

The input parameters are:

The number of sampled points for FFT	512 points
Sampling interval	
Time domain	0.002 sec
Frequency domain	1/(512 x 0.002) hz
Operator length	
Time domain	151 points
Frequency domain	512 points
White noise	0.01%

From Figures 13 and 18, we can observe that the high-frequencies attenuated by the array responses can be restored. Figures 14, 15, 19, and 20 indicate that the deconvolved wavelet, for each array response of case 2 or case 3, has a time lead which is equal to half of the duration of the corresponding array response.

Discussion of the Results in Part B

1) The restoration of the bandwidth

The signal impinging upon the arrays convolves with the array responses having the pass-bands shown in Figures

8 and 9 for the specified phase velocities. Thus, the high-frequency signal compontns within the pass-band of the recording filter (Figure 10) will be attenuated and inverted in sign by the array responses and will not be used effectively. Now, comparing the amplitude spectra in Figures 10, 11, and 12 before deconvolutions with those in Figures 13 and 18 after deconvolutions, we can observe that the bandwidth outside the central pass-band of the array has been restored by applying the minimum-phase deconvolution techniques. Experience has taught us that the restoration increases with decreasing white noise constant. In order to prevent the divergence of $\log|H(k)|$ associated with zeros of H(z) on the unit circle, we added the white noise constant to $\log|H(k)|$. Hence, the white noise will influence the computed phase, just as it did during the time-domain operator design; however, colored noise could have been used here.

2) The time shift due to the deconvolutions

From Figures 14 and 15, it can be seen that the deconvolved wavelets obtained by using the Hilbert transform have time leads. From the appropriate phase curve (e.g., Figure 16) these leads were measured as 1 ms for the array of Case 2 and 3 ms for case 3. Each time lead in the output is equal to half of the duration of the array response.

What causes the time leads? Each input wavelet (Figure 11 or 12) is the convolution of the array response a(n) with

the minimum-phase recording filter i(n)(Figure 10). Taking the even element cases computed in the thesis for example, we have

$$\begin{matrix} a(n) & * & i(n) \\ |A(k)| & & |I(k)| \end{matrix} \quad \exp\, j[\theta_I(k) + p \pm \pi k \Delta f \Delta\tau], \qquad (16)$$

where $|A(k)|$ is the Fourier amplitude spectrum of the array response, $|I(k)|$ and $\theta_I(k)$ are the amplitude and phase spectra of the instrument filter.

After taking the logarithm of the convolved amplitude spectrum and passing it through the Hilbert transform, we have

$$\log\, [\, |A(k)| \cdot |I(k)| \,] * V_N(k) = \theta_A(k) + \theta_I(k)$$

where $\theta_A(k) = \log |A(k)| * V_N(k) \neq p \pm \pi k \Delta f \Delta\tau$.

Note that $\theta_A(k)$ is a minimum phase computed from the logarithm of the array amplitude.

After convolving the input spectra (Equation (16)) with the frequency-domain inverse filter

$$\frac{1}{|A(k)|\ |I(k)|} \exp\, [-j(\theta_A(k) + \theta_I(k))],$$

we will obtain the deconvolved output

$$\exp\, [-j\ (\theta_A(k) + p \pm \pi k \Delta f \Delta\tau)]\ .$$

The phase term $\theta_A(k)$ has a linear phase component (Fig. 23) which gives the time lead in the output pulse. $\theta_A(k)+\pi k\Delta f\Delta\tau$ gives a total linear phase shift in the output (Fig. 16).

Also, Figures 19 and 20 indicate that the deconvolved wavelets obtained by applying the one-sided least-squares operator to the arrays of Case 2 and 3 have lead times the same as those obtained by using the Hilbert transform. The operator derived by solving the normal equations (1) and (1-1) cannot be zero-phase due to its causality. For the symmetric input array response, the causal operator provides a minimum phase, which turns out to be nearly linear, with a slope affording the time lead in the output.

Many seismic velocity estimation techniques utilize the variation of normal moveout with travel time. Most of the techniques assume stacking velocity, apply the normal moveouts corresponding to the offsets of CDP traces, and then measure the coherence among the traces. The time leads caused by the minimum-phase deconvolutions may distort the normal moveout curve, and cause errors in estimating velocity.

COMPUTER TIME COMPARISON BETWEEN THE TWO METHODS

The computer time required for each method depends on the inputs and the outputs, such as the length of input wavelet, the selected parameters, and the plotted figures. For the programs used in the study, the CPU time (CSM PDP-10 Computer) needed to compute and plot the results shown in Figure 7B, using the Hilbert transform, is 49.04 seconds; that needed to compute and plot the results shown in Figure 7C, using the Levinson's algorithm, is 63.84 seconds. Hence, the frequency-domain deconvolution using the Hilbert transform was slightly faster in this test. In general, the author's impression is that the times are comparable.

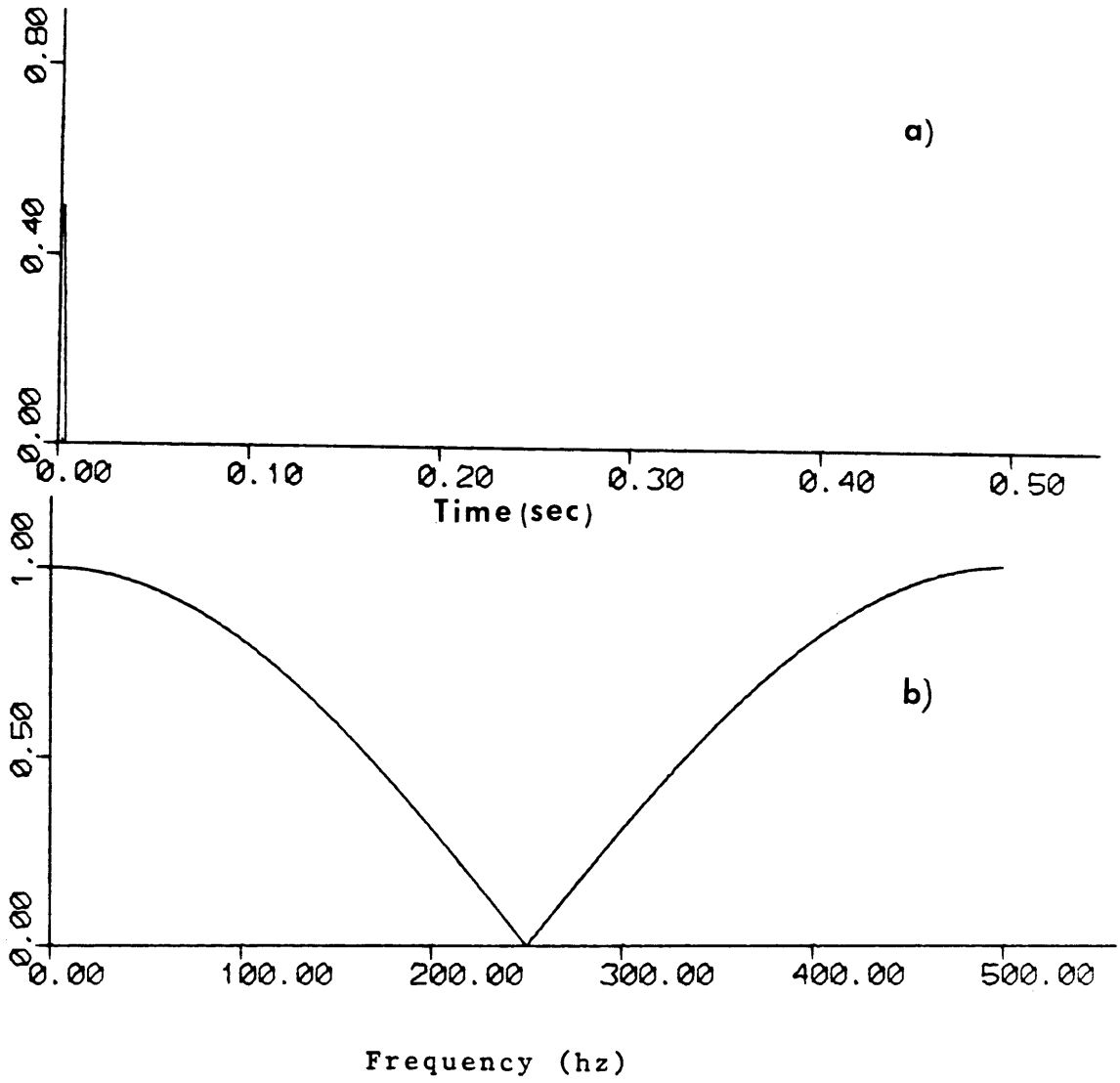

Figure 8 . a) Receiver array response $a_2(t)$ and b) amplitude spectrum.

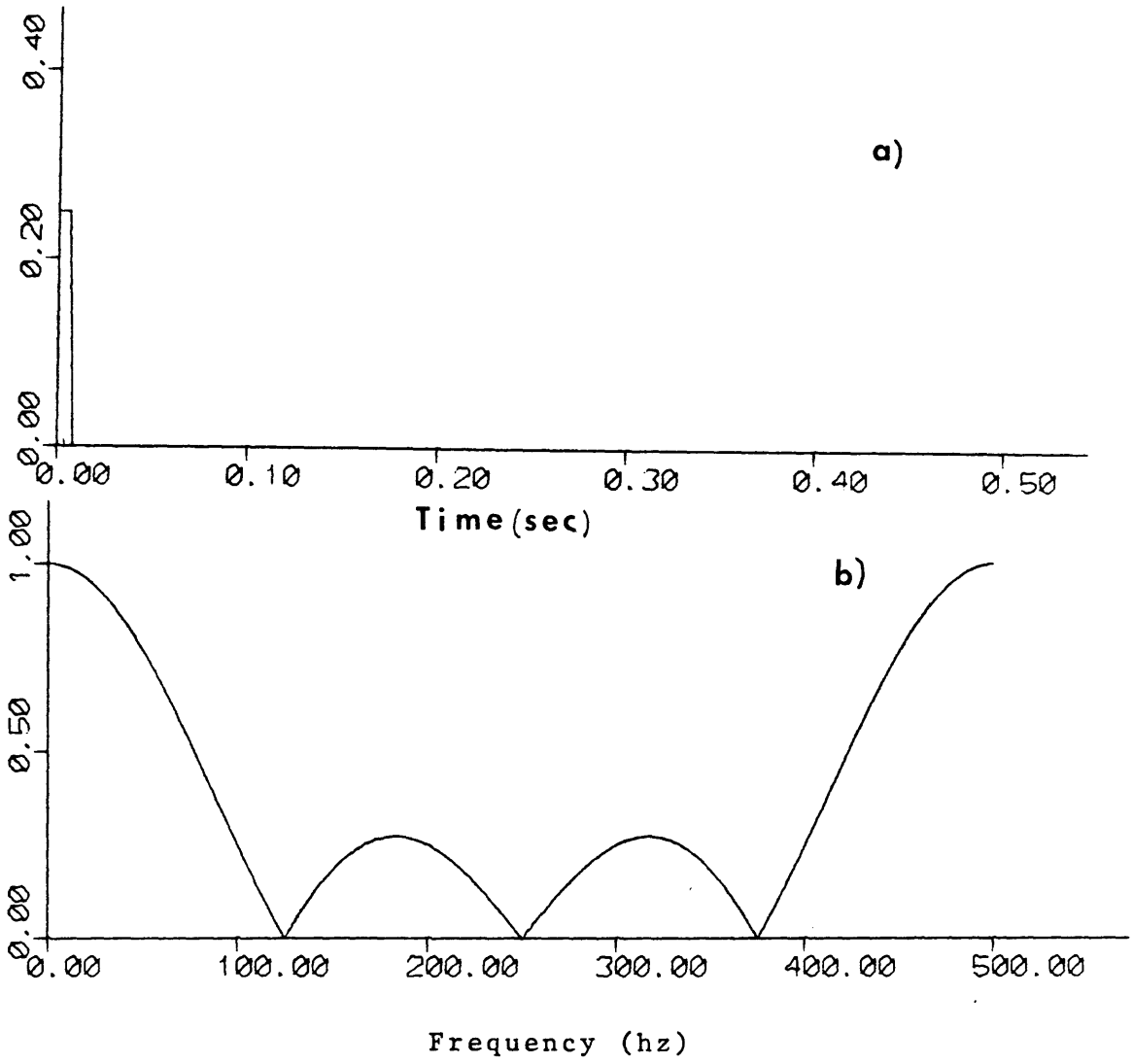

Figure 9 . a) Receiver array response, $a_3(t)$, and b) amplitude spectrum.

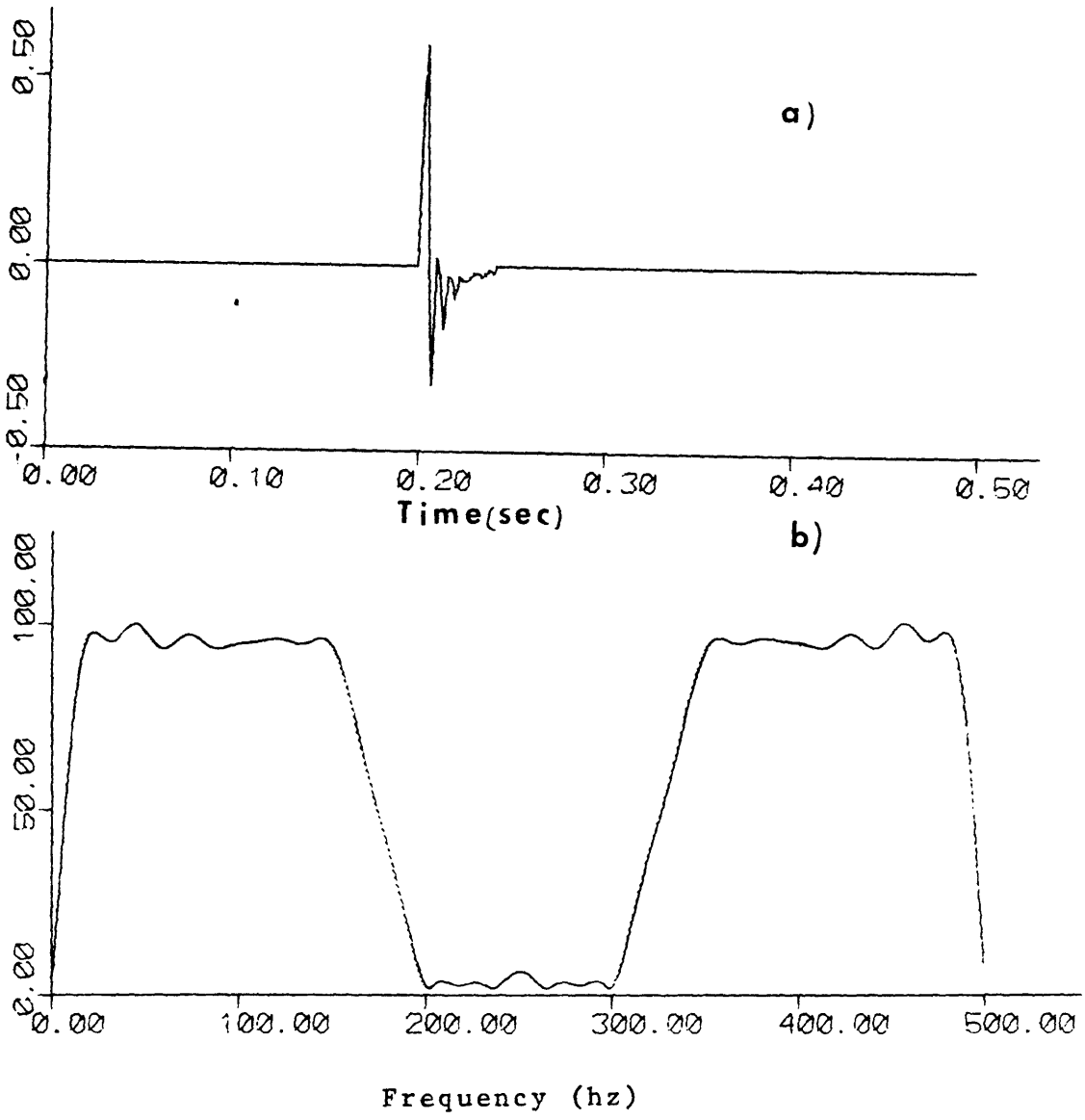

Figure 10. Recording filter (15/18-150 hz).
a) Impulse response and b) amplitude spectrum.

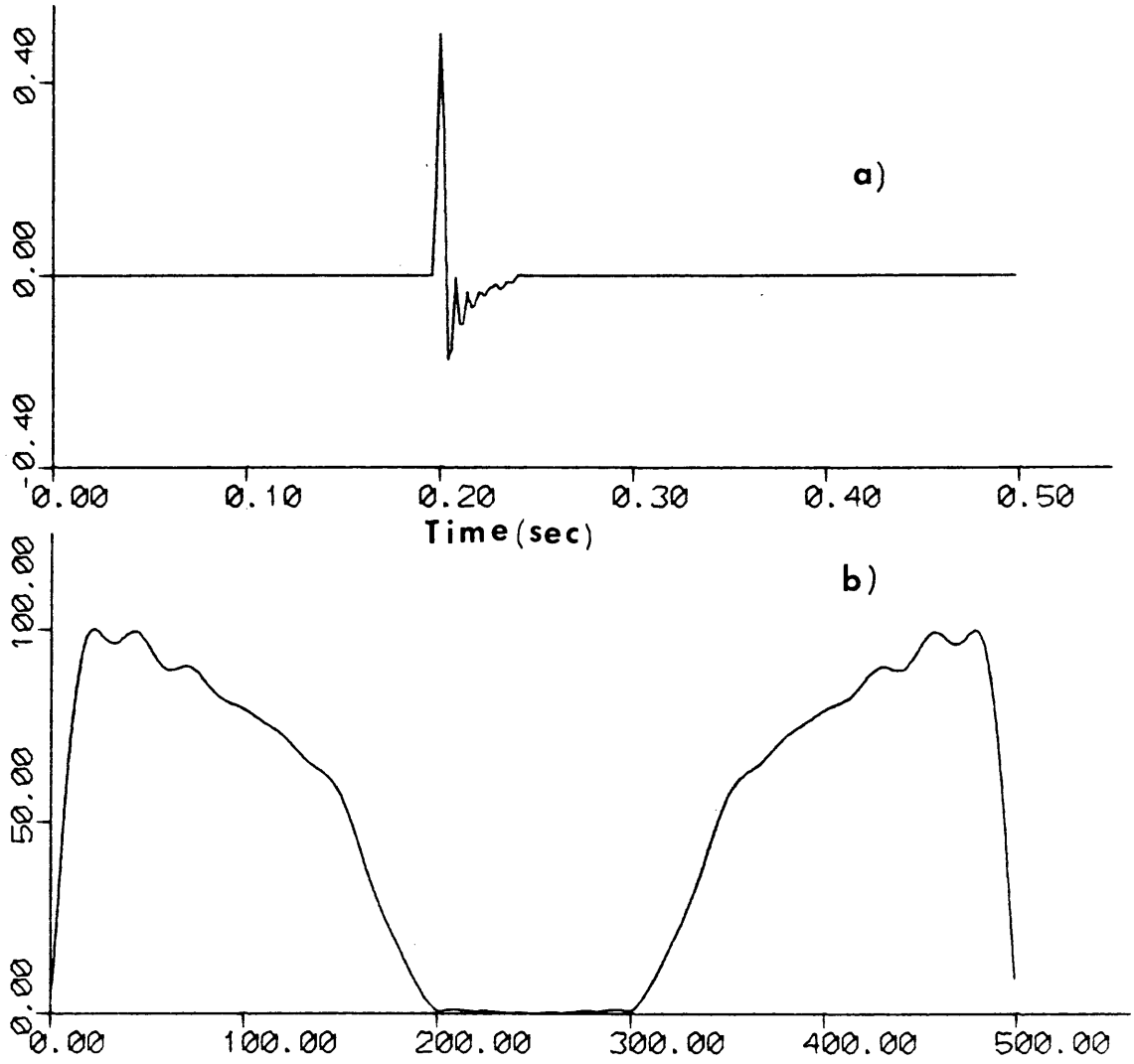

Figure 11. The Convolution of the recording filter in figure 10 and the array response $a_2(t)$. a) Impulse response and b) Amplitude spectrum.

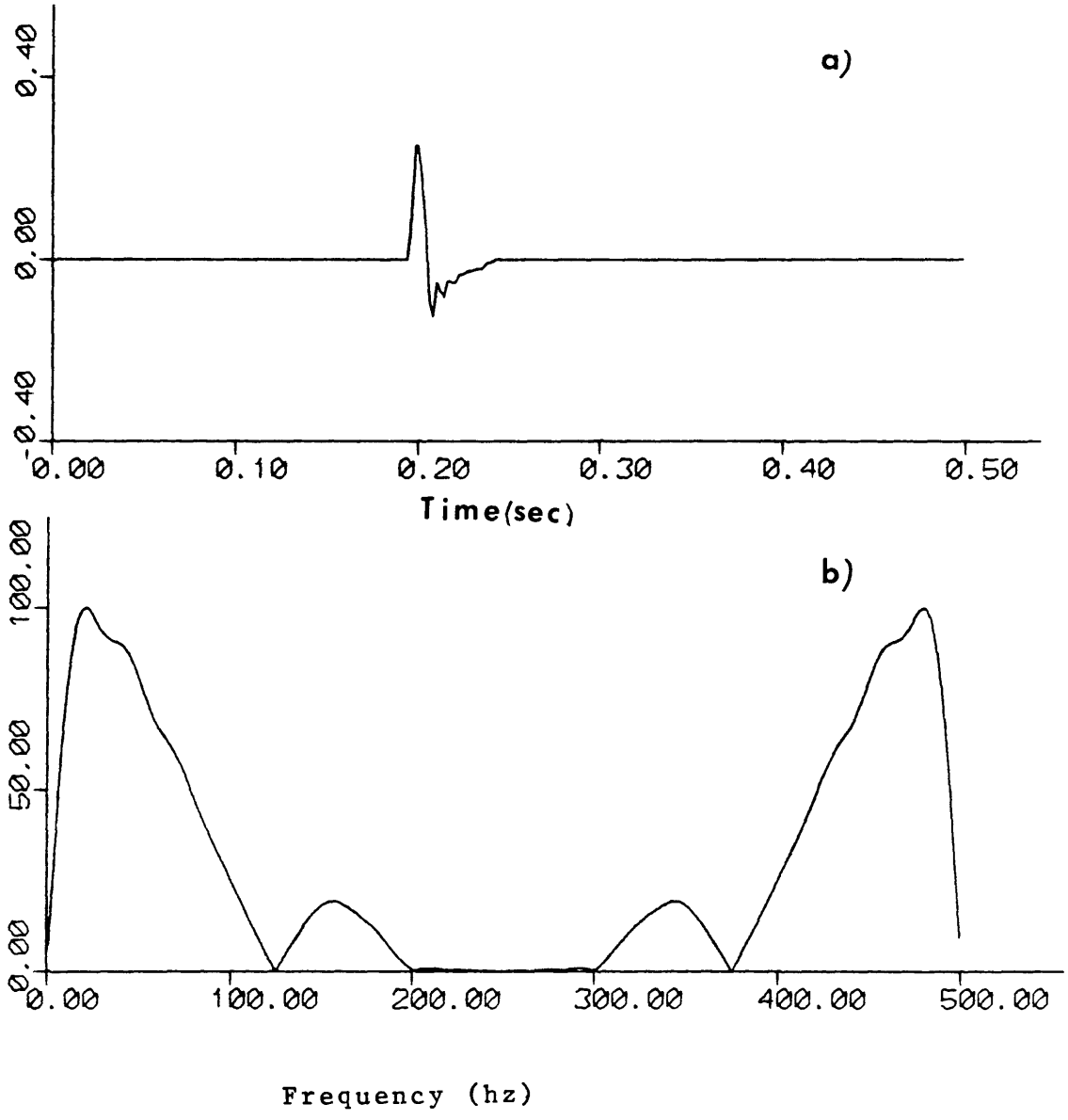

Figure 12. The Convolution of the recording filter in Figure 10 and the array response $a_3(t)$, a) Impulse response and b) amplitude spectrum

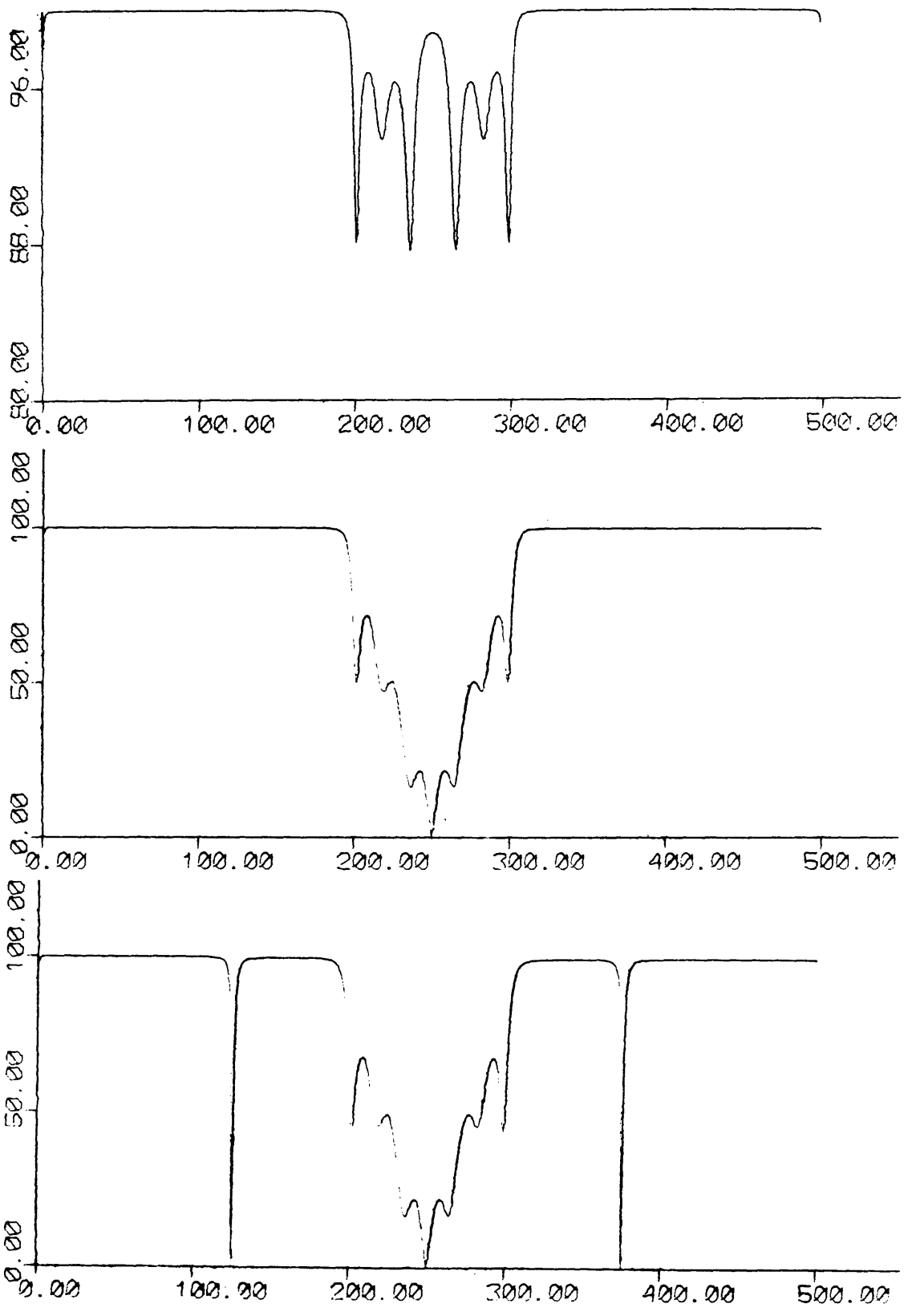

Figure 13. Deconvolved amplitude spectra of the three inputs in Figures 10 to 12, White noise 0.0001, by the Hilbert transform.

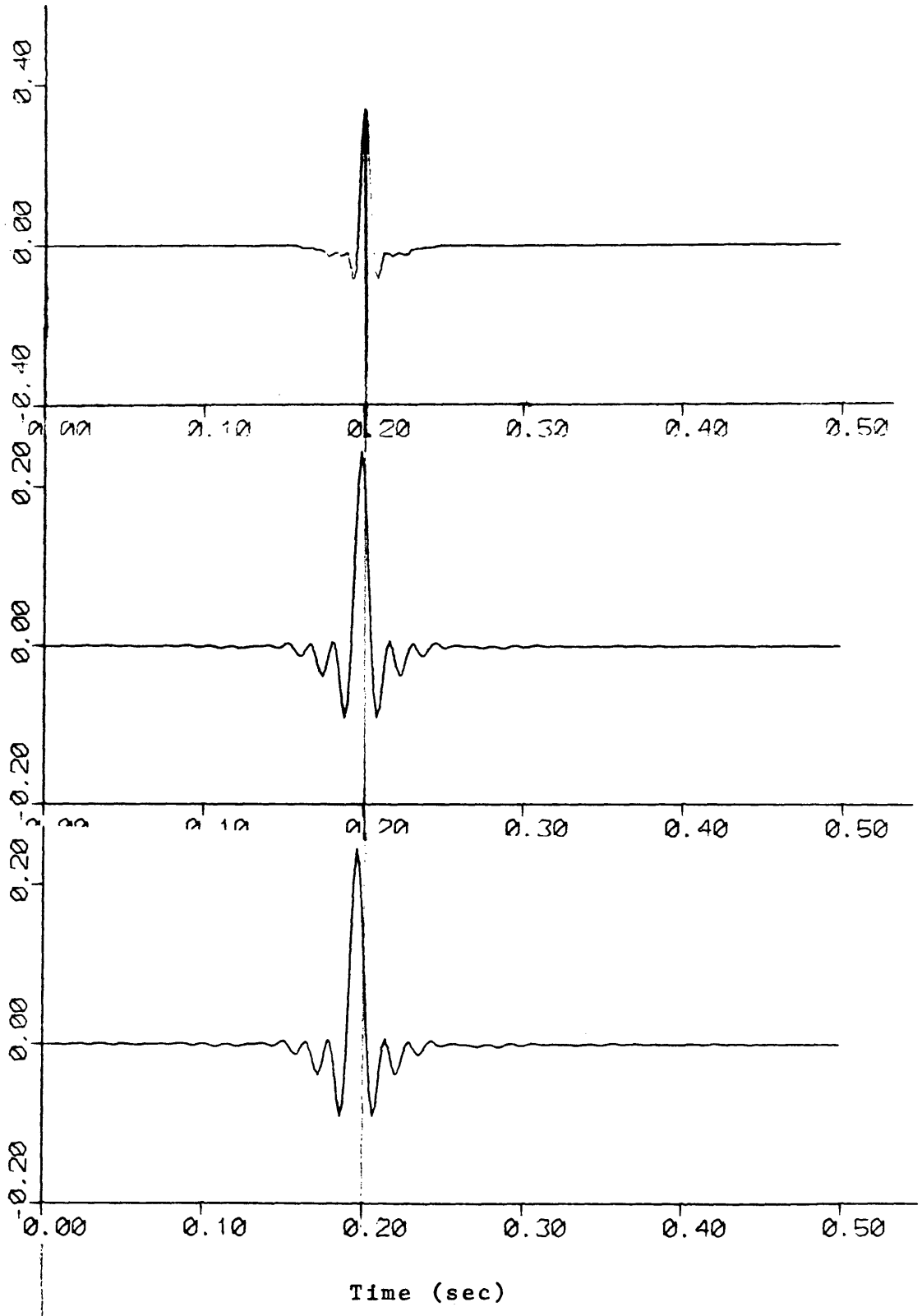

Figure 14. Deconvolved wavelets of the three inputs in figures 10 to 12, band-pass filter 18-62 hz, by the Hilbert transform.

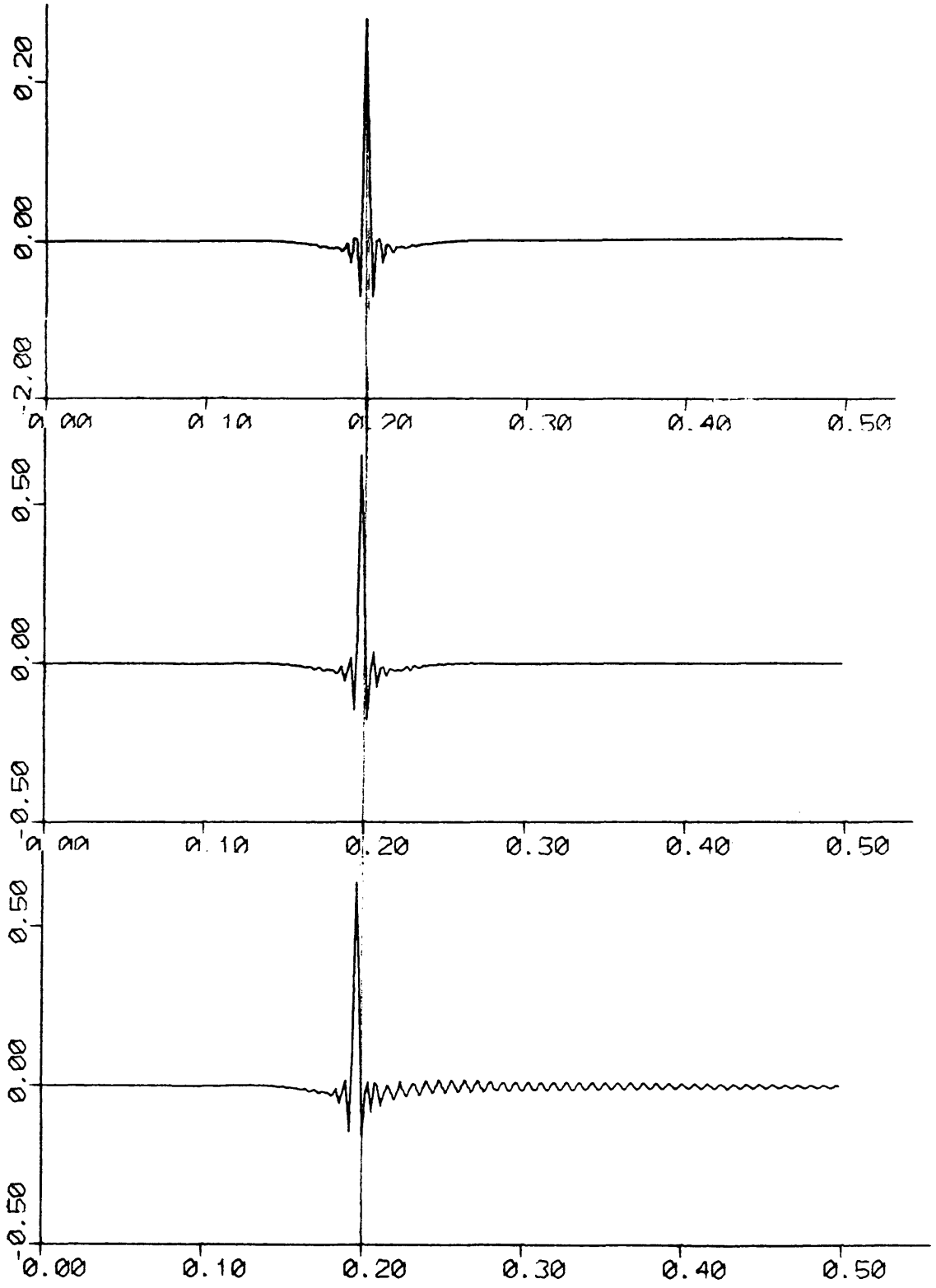

Figure 15. Deconvolved wavelets of the three inputs in Figures 10 to 12, band-pass filter 15-150 hz, by the Hilbert transform.

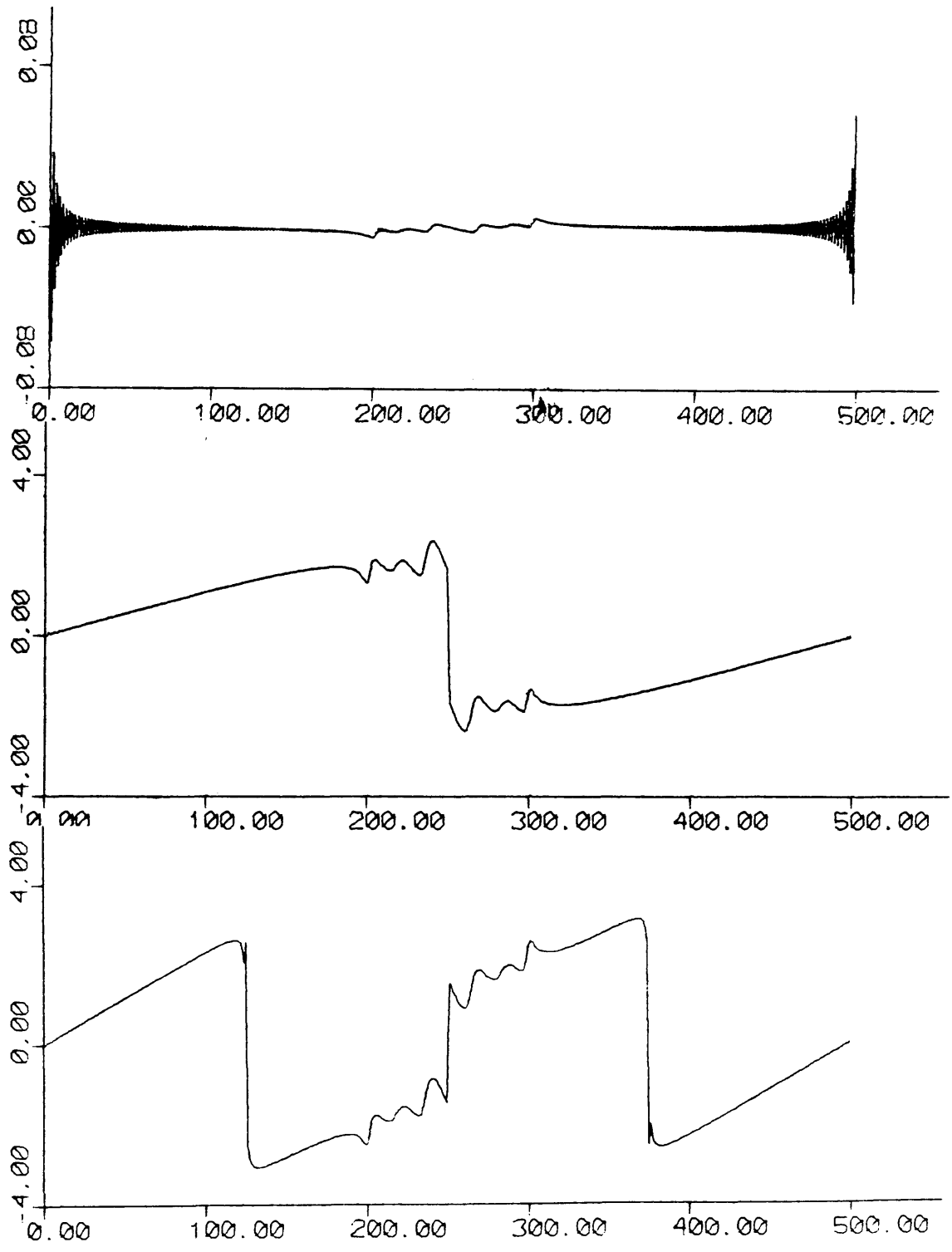

Figure 16. Deconvolved phase of the three inputs in Figures 10 to 12, by the Hilbert transform.

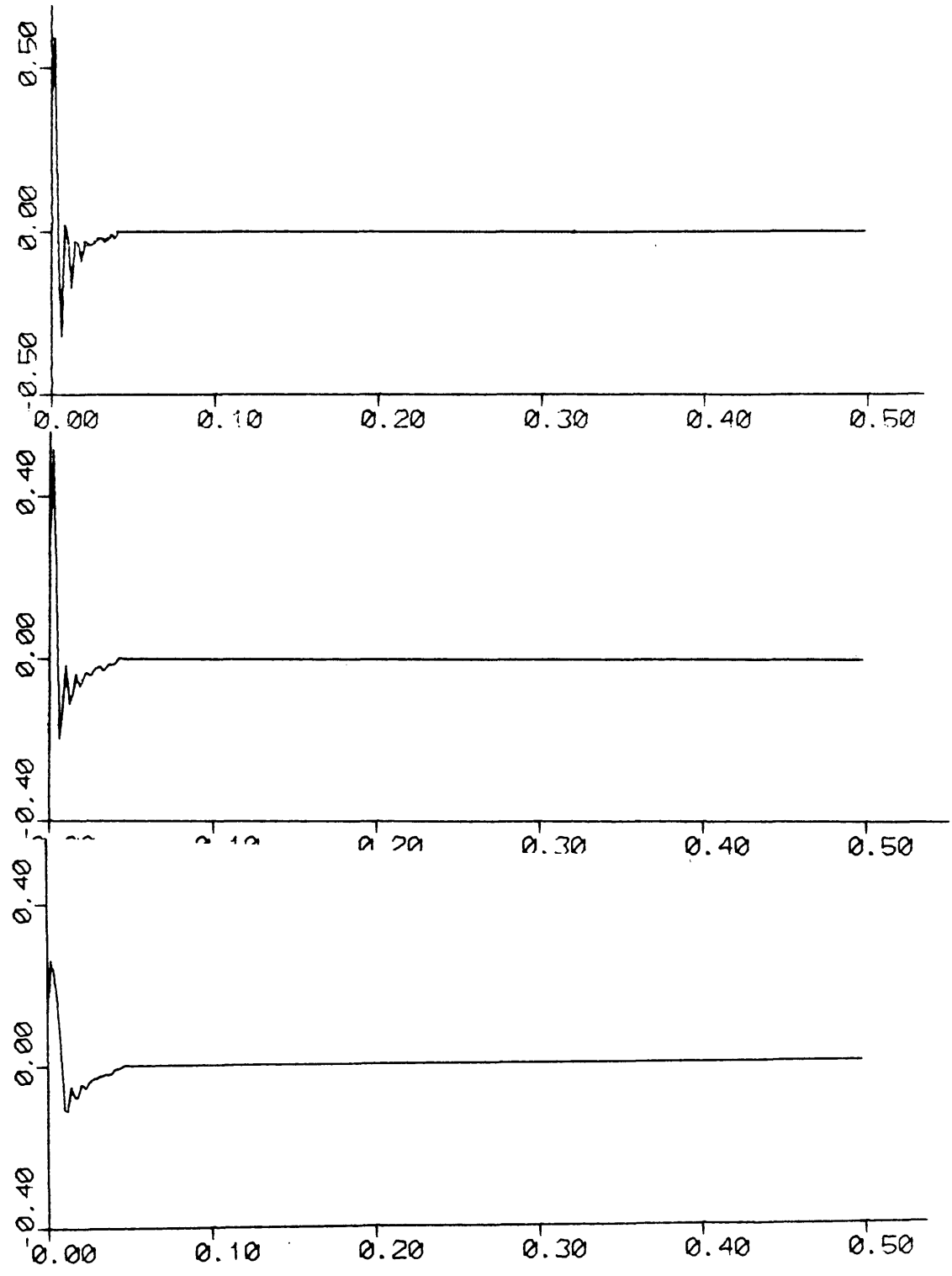

Figure 17. Estimates of the three inputs in Figure 10 to 12, by the Hilbert transform.

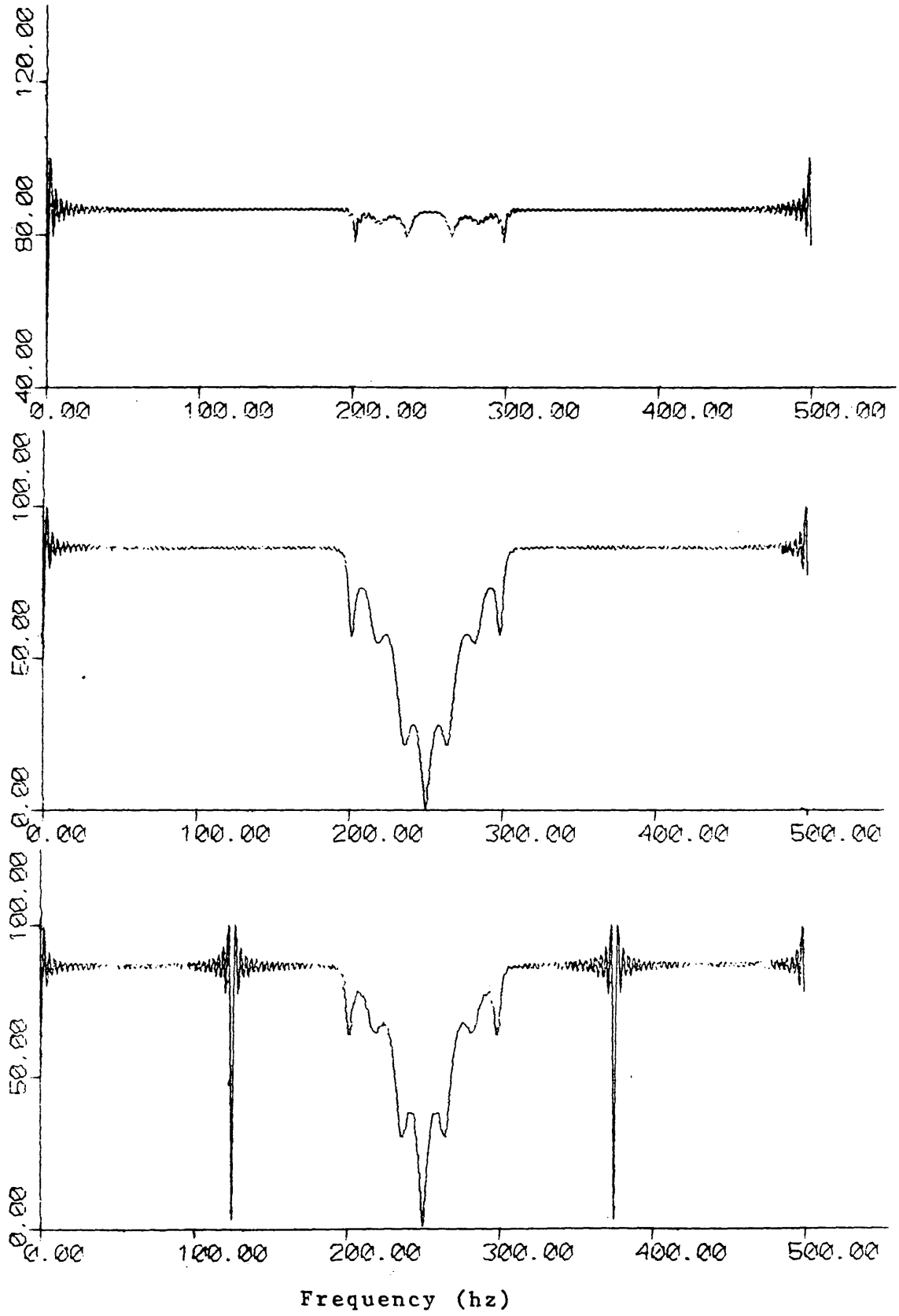

Figure 18. Deconvolved amplitude spectra of the three inputs in Figures 10 to 12, white noise 0.0001, by the time-domain deconvolution.

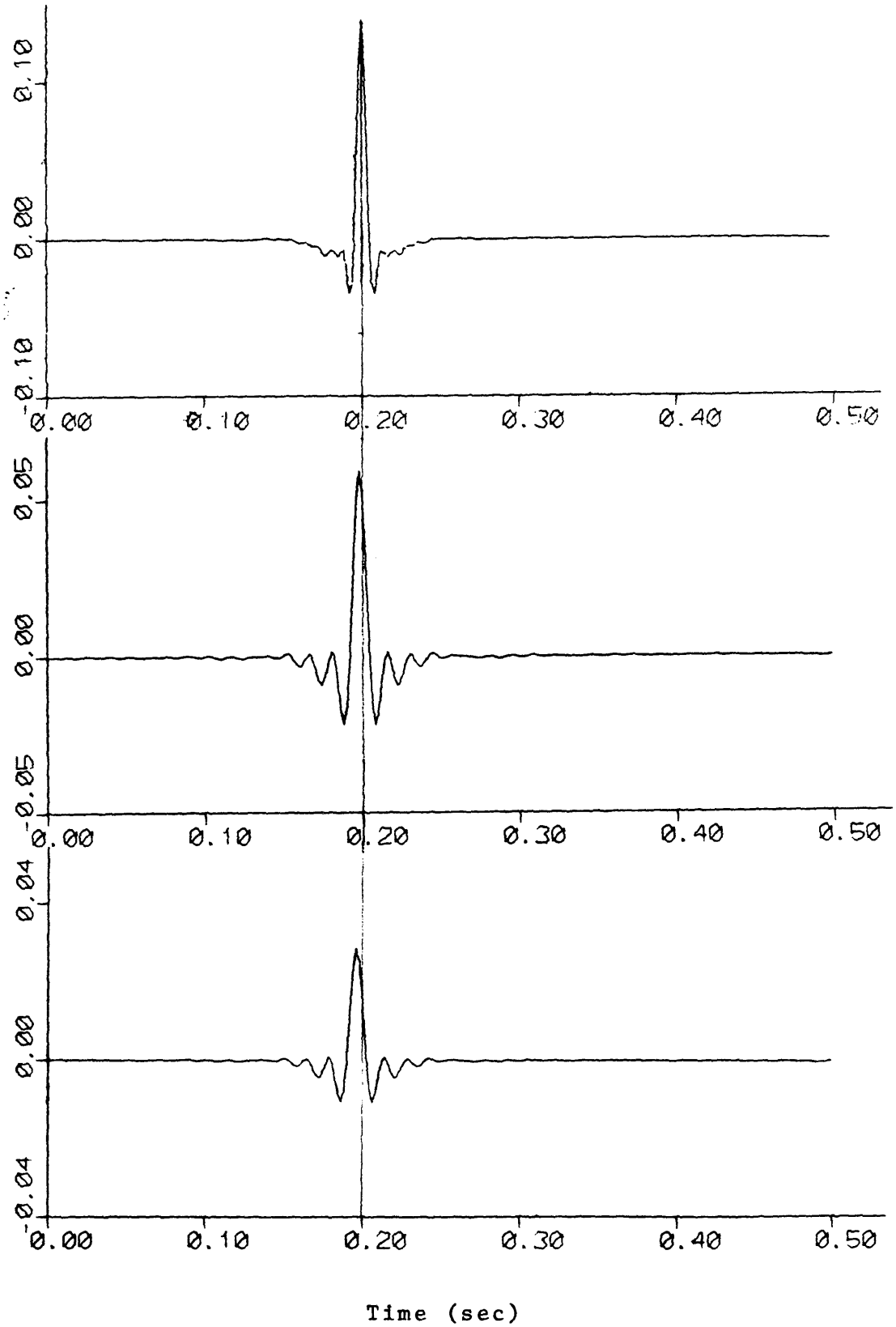

Figure 19. Deconvolved wavelets of the three inputs in Figures 10 to 12, band-pass filter 18-62 hz, by the time domain deconvolution.

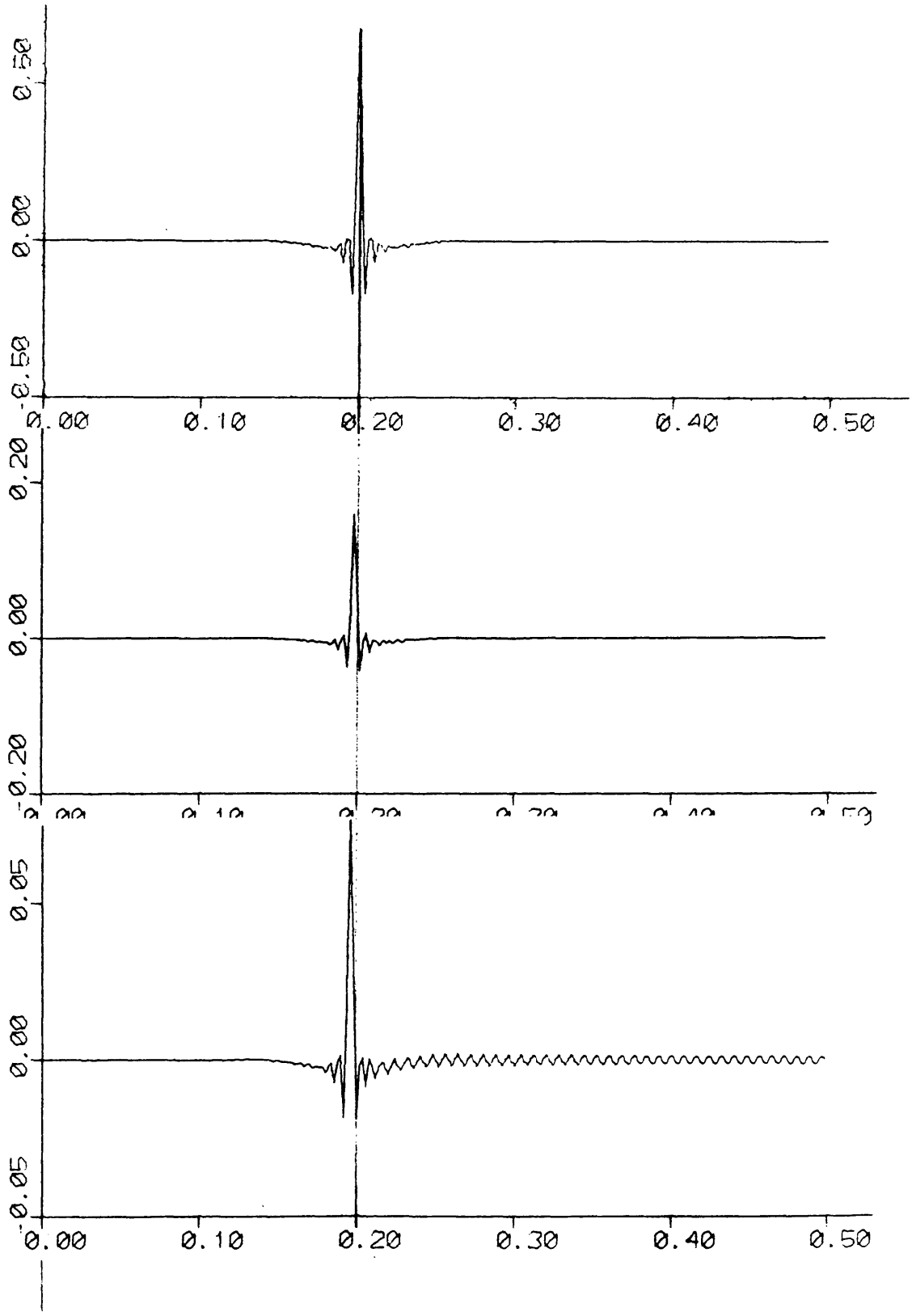

Figure 20. Deconvolved wavelets of the three inputs in Figures 10 to 12, band-pass filter 15-150 hz, by the time-domain deconvolution.

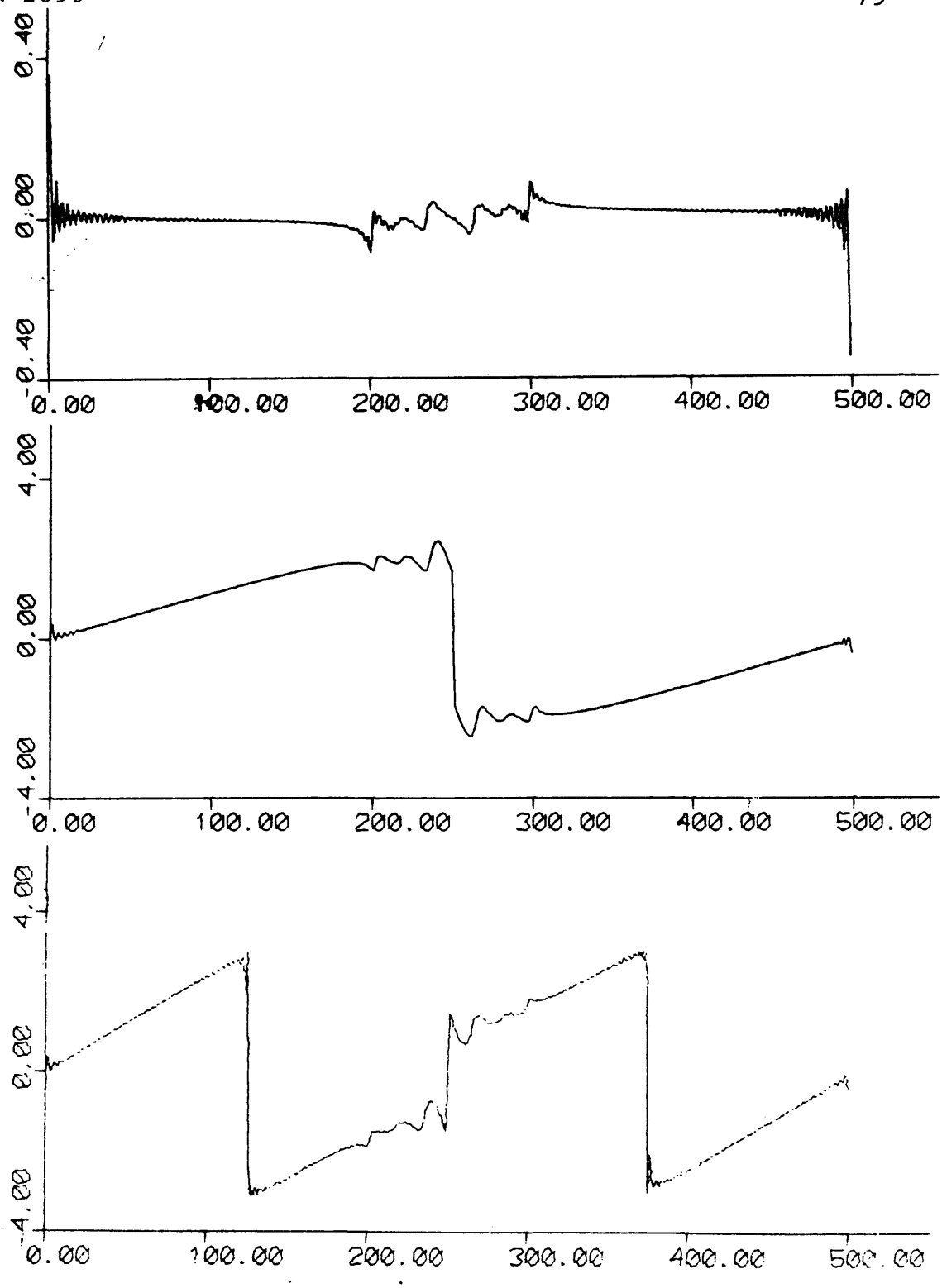

Figure 21. Deconvolved phase of the three inputs in Figures 10 to 12, by the time-domain deconvolution.

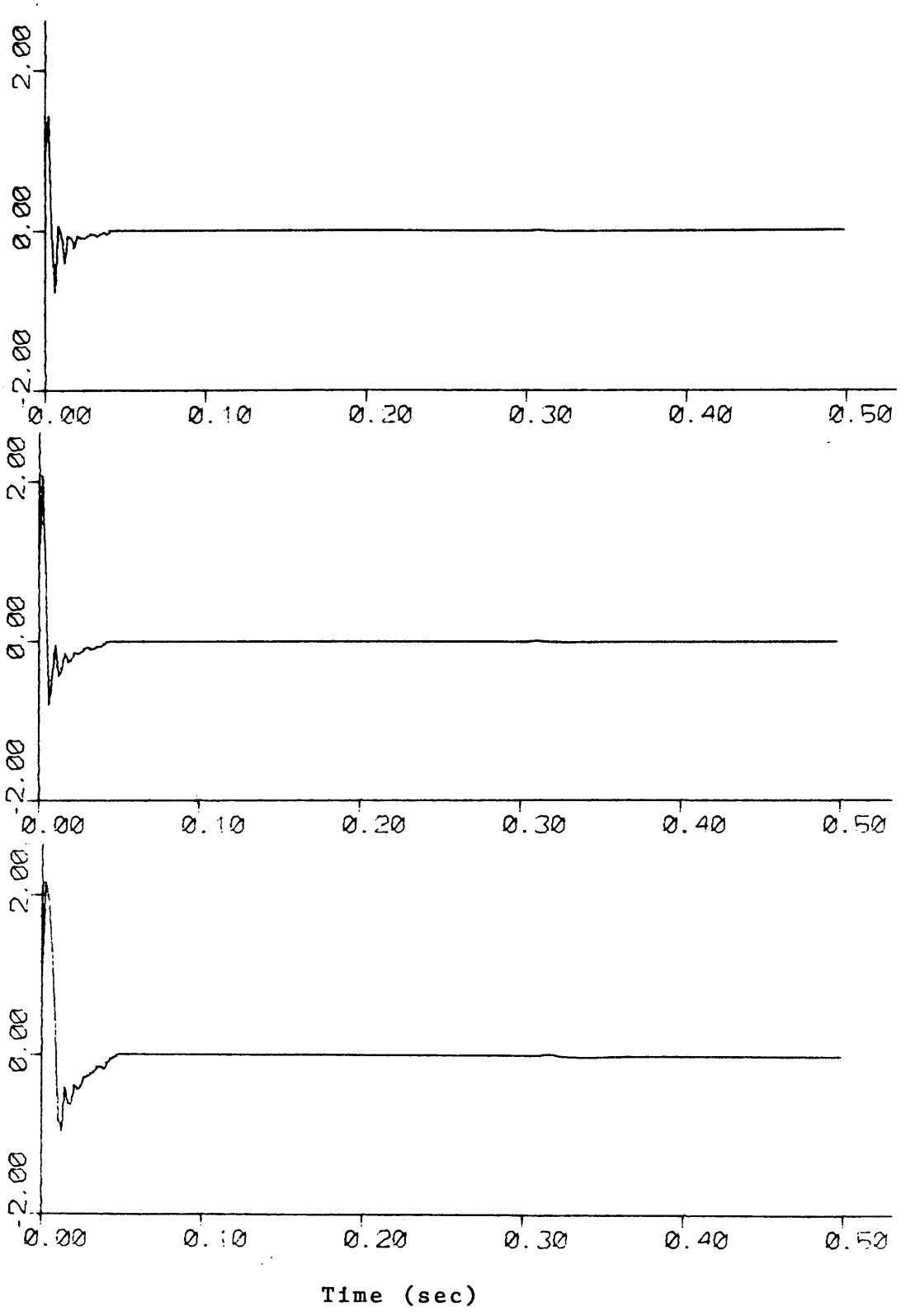

Figure 22. E estimates of the three inputs in Figures 10 to 12, by the time-domain deconvolution.

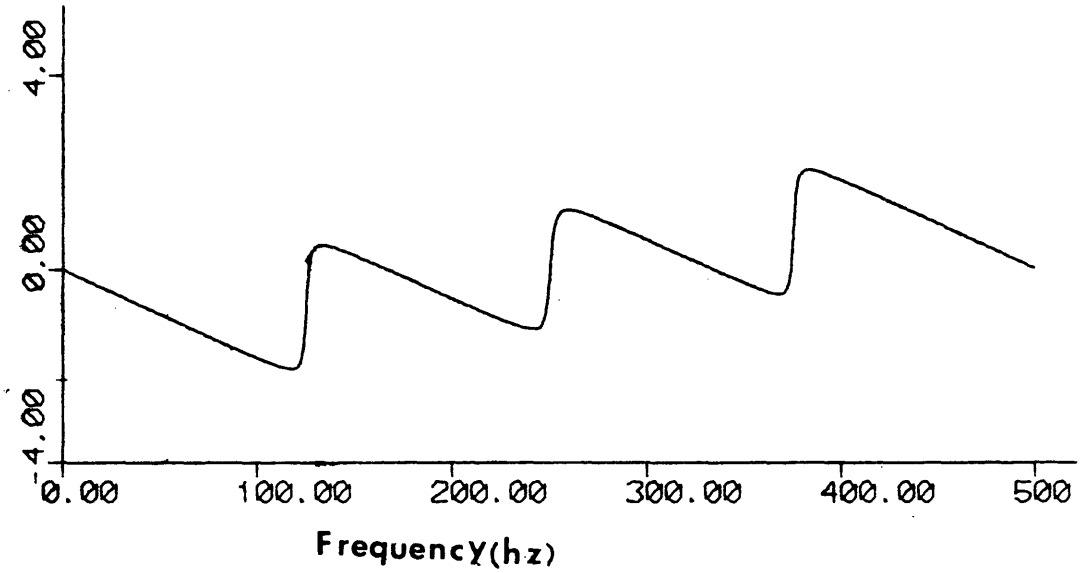

Fig. 23. The phase curve $\theta_A(k)$ of the array response $\mathbf{a}_3(t)$, computed by the Hilbert transform, white noise 0.0001.

CONCLUSIONS

1. The minimum-phase assumption should be met by the two deconvolution approaches in order to produce a zero-phase or symmetric output pulse.

2. The minimum-phase deconvolution based on the Hilbert transform in the frequency-domain is more suitable for seismic wavelet processing than the one-sided least-squares algorithm. In operator design using the Hilbert transform, one can add white noise to the input amplitude spectrum without affecting the computed minimum phase. This is not possible when the Levinson's technique is employed.

3. Both deconvolution techniques can restore the band-width outside the central pass-band of the receiver array, but both produce a time lead in the deconvolved wavelet which is due to the non-minimum phase of the array. The time lead is equal to half of the duration of the array response. The time lead may cause error in estimating velocity due to the distortion of moveout curve.

4. In general, the computing times needed for the two methods are comparable. For some cases, the Hilbert transform method is slightly faster than the least-squares method.

REFERENCES

Berkhout, A.J., 1977, Least-squares inverse filtering and wavelet deconvolution: Geophysics, v. 42, no. 7, p. 1369-1383.

Claerbout, J.F., 1976, Fundamentals of Geophysical Data Processing, McGraw Hill, New York.

Galbraith, J.N., 1971, Prediction error as a criterion for operator length: Geophysics, v. 36, n. 2, p. 261-265.

Levinson, N., 1946, The Wiener RMS error criterion in filter design and prediction: Math. Phys. 25, p. 261-278.

Lindseth, R.O., 1973, Recent advances in digital processing of geophysical data: SEG Continuing Education.

Lines, L.R., and Ulrych, T.T., 1977, The old and the new in seismic deconvolution and wavelet estimation: Geophysical Prospecting, v. 25, no. 3, p. 512-533.

Oppenheim, A.V., and Schafer, R.W., 1975, Digital Signal Processing, Prentice-Hall, Inc., Englewood Cliffs, N.J.

Papoulis, Athanasios, 1968, Systems and Transforms with Applications in Optics: McGraw-Hill.

Peacock, K.L., and Treitel, Sven, 1969, Predictive deconvolution: Theory and practice: Geophysics, v. 34, no. 2, p. 155-169.

Robinson, E.A., 1957, Predictive decomposition of seismic traces: Geophysics, v. 22, p. 767-778.

_____, 1967, Prediction decomposition of time series with application to seismic exploration: Geophysics, v. 32, p. 418-484.

_____, 1967, Multichannel Time Series Analysis with Digital Computer Programs, San Francisco, Holden-Day.

Robinson, E.A., and Treitel, S., 1967, Principles of digital Wiener filtering: Geophysical Prospecting, v. 15, p. 311-333.

Schneider, W.A., 1977, Wavelet processing: SEG Continuing Education.

Schoenberger, M., 1974, Resolution comparison of minimum-phase and zero-phase signals: Geophysics, v. 39, no. 6, p. 826-833.

_____, 1970, Optimization and impliementation of marine seismic arrays: Geophysics, v. 35, no. 6, p. 1038-1053.

APPENDIX

THE COMPUTER PROGRAMS AND USER'S MANUAL

(Retained in Geophysics Department Library)